TECTONICS, VOL. 32, 216–238, doi:10.1002/tect.20029, 2013

Latest Quaternary paleoseismology and slip rates of the Longriba fault zone, eastern Tibet: Implications for fault behavior and strain partitioning

Junjie Ren,[1,2,3] Xiwei Xu,[2] Robert S. Yeats,[3] and Shimin Zhang[1]

Received 12 September 2012; revised 13 January 2013; accepted 3 February 2013; published 29 April 2013.

[1] Although much work has been done on active tectonics of eastern Tibet, little is known about the Longriba fault zone and its role in strain partitioning. Whether its two sub-parallel strands (Longriqu and Maoergai faults) can rupture simultaneously in a large earthquake remains unknown. We conducted trenching combined with the interpretation of satellite imagery, field investigations, topographic surveys, and radiocarbon and Optically Stimulated Luminescence (OSL) dating to reconstruct paleoseismic history, and we used displaced terrace risers to estimate geological slip rates. Our results demonstrate that the Longriba fault zone is predominantly right-lateral with a small southeast-verging thrust component. Four surface-rupturing events occurred on the Longriqu fault at 5080 ± 90, 11,100 ± 380, 13,000 ± 260, and 17,830 ± 530 cal yr B.P. Together with our previous trenches on the Maoergai fault, we found that the last event probably ruptured both the Longriqu and Maoergai faults. Prior to the last event, the two strands of the Longriba fault zone experienced alternating earthquakes. The fault zone has a high potential for an earthquake larger than Mw 7. The slip rate of the Longriba fault zone decreases from ~7.5 mm/yr in latest Pleistocene to ~2.1 mm/yr in the Holocene, probably related to a slowing down of the eastern motion of the Tibetan Plateau. The comparison with slip rates at the Longmen Shan fault zone suggests that the Longriba fault zone has an equally important role in strain partitioning in eastern Tibet. This study is helpful to seismic hazard assessment and an understanding of deformation mechanism in eastern Tibet.

Citation: Ren, J., X. Xu, R. S. Yeats, and S. Zhang (2013), Latest Quaternary paleoseismology and slip rates of the Longriba fault zone, eastern Tibet: Implications for fault behavior and strain partitioning, *Tectonics*, *32*, 216–238, doi:10.1002/tect.20029.

1. Introduction

[2] The ongoing collision between the Indian and Eurasian plates has led to the eastward extrusion of the Tibetan Plateau [*Molnar and Tapponnier*, 1975; *Peltzer and Saucier*, 1996; *Tapponnier and Molnar*, 1977; *Zhang et al*., 2004], accompanied by uplift in eastern Tibet, where the Longmen Shan rises 6000 m above the Sichuan Basin, exhibiting greater relief than anywhere else on the Plateau (Figure 1). A lower crustal flow model [*Bird*, 1991; *Clark and Royden*, 2000; *Royden et al*., 2008] in which low-viscosity material in the lower crust extrudes outward from the interior Plateau and inflates the crust beneath the Longmen Shan (shan means range) was proposed to illustrate the low rate of east-west shortening across the range and within the basin inferred from geodetic measurements and geomorphic investigations [*Densmore et al*., 2007; *Li et al*., 2006; *Ma et al*., 2005; *Shen et al*., 2005; *Zhang et al*., 2004]. Conversely, some studies argued that the thickening of brittle crust [*Hubbard and Shaw*, 2009; *Lease et al*., 2012; *Tapponnier et al*., 2001; *Xu et al*., 2009] associated with thrust faults rooted in the lithosphere with large amounts of slip is completely responsible for uplift of eastern Tibet . Although much work has been conducted on the Longmen Shan fault zone [summary by *Zhang*, 2013], especially since the 2008 Wenchuan earthquake (Mw 7.9), the mechanism causing high elevation and thick crust in eastern Tibet remains debatable. In both models, Tibet was regarded to move eastward relative to the Sichuan Basin across a wide area without identifiable faults, and the strain in eastern Tibet was accommodated dominantly by the Longmen Shan fault zone. Accordingly, the role of the Longriba fault zone in these two scenarios was neglected.

[3] The Longriba fault zone, ~200 km west of the Longmen Shan, is parallel to the Longmen Shan fault zone and separates the Bayan Har block (also called Songpan-Ganzi block) into the Aba (sub-block 1 in Figure 1b) and

[1]Key Laboratory of Crustal Dynamics, Institute of Crustal Dynamics, China Earthquake Administration (CEA), Beijing, China.
[2]Key Laboratory of Active Tectonics and Volcano, Institute of Geology, China Earthquake Administration (CEA), Beijing, China.
[3]College of Earth, Ocean, and Atmospheric Sciences, Oregon State University, Corvallis, Oregon, USA.

Corresponding author: J. Ren, Institute of Crustal Dynamics, China Earthquake Administration, Xisanqi, Haidian, PO Box 2855, Beijing 100085, China. (renjunjie@gmail.com)

0278-7407/13/10.1002/tect.20029

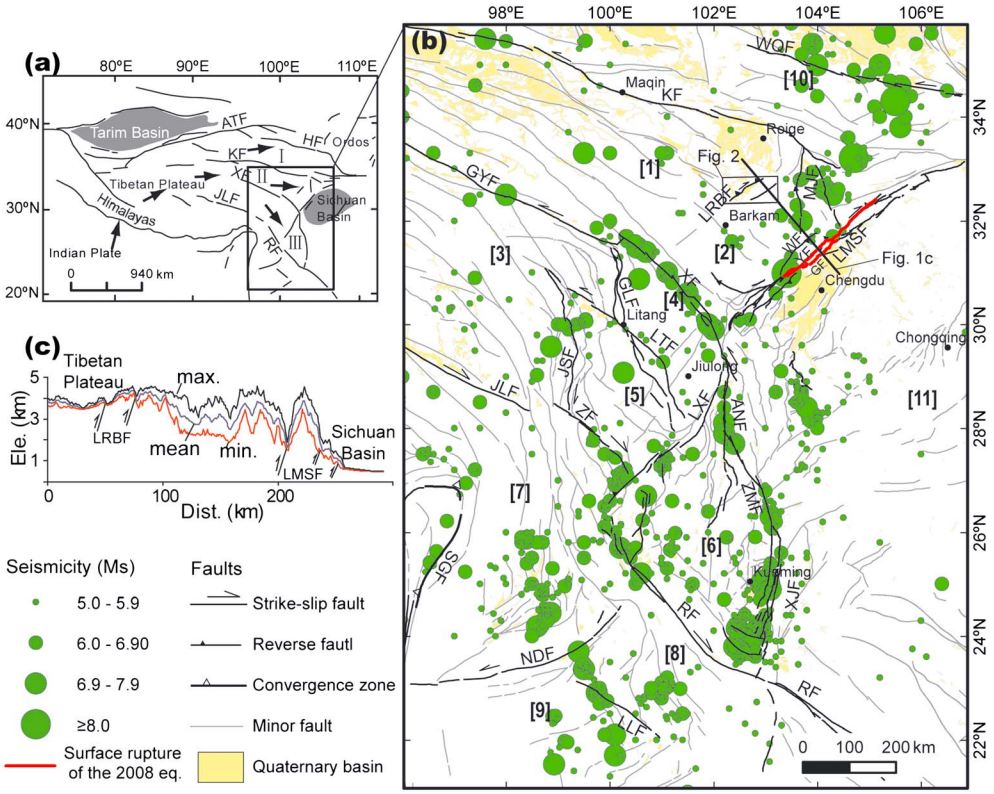

Figure 1. Tectonic setting of the Longriba fault zone in eastern Tibet. (a) Major boundary faults and blocks of the Tibetan Plateau. Black arrows indicate block motion direction according to GPS data [*Gan et al*., 2007]. I, Qaidam-Qilian block; II, Bayan Har block; III, Sichuan-Yunnan block. (b) Active faults and seismicity in eastern Tibet showing several rigid sub-blocks. Seismic data include instrumentally recorded earthquakes [China Earthquake Networks Center, http://www.csndmc.ac.cn/newweb/data.htm] and historical earthquakes [*China Earthquake Administration*, 1999a, 1999b]. Fault data are modified after *Xu et al*. [2008]. Surface ruptures of the 2008 Wenchuan earthquake are according to *Xu et al*. [2009]. Eastern Tibet and adjacent regions are divisible into 11 sub-blocks [*Cheng et al*., 2012]: 1, Aba; 2, Longmen Shan; 3, Zangdong; 4, Yajiang; 5, Shangri La; 6, Dianzhong; 7, Baoshan; 8, Jinggu; 9, Ximen; 10, Western Qinling; 11, South China. (c) Swath profile across the Longriba and Longmen Shan fault zones. See location in Figure 1b. Abbreviations for active faults: ANF, Anninghe fault; ATF, Altyn Tagh fault; GF, Guanxian-Jiangyou fault; GLF, Ganze-Litang fault; GYF, Ganze-Yushu fault; HF, Haiyuan fault; JLF, Jiali fault; JSF, Jinshajiang fault; KF, Kunlun fault; LLF, Longling-Lancang fault; LMSF, Longmen Shan fault; LRBF, Longriba fault; LTF, Litang fault; LXF, Lijiang-Xiaojin fault; MJF: Minjiang fault; NDF, Nandinghe fault; RF, Red River fault; SGF, Sagaing fault; WF, Wenchuan-Maoxian fault; WQF, Western Qinling fault; XF, Xianshuihe fault; XJF, Xiaojiang fault; YF, Yingxiu-Beichuan fault; ZF, Zhongdian fault; ZMF, Zemuhe fault.

Longmen Shan sub-blocks (sub-block 2 in Figure 1b). The Aba sub-block is characterized by a series of northwest-trending left-lateral strike-slip faults, accompanying the eastward motion of the Bayan Har block. In contrast, the Longmen Shan sub-block is marked by strong shortening and mountain building, accompanying northeast- to nearly north-south-striking large-scale thrust faults and related folds. The Longriba fault zone was first described as a dextral shear zone inferred from GPS measurement [*Shen et al*., 2005]. However, little is known about the late Quaternary activity of the Longriba fault zone, and even its active-fault pattern is still unclear. Some researchers proposed predominantly normal faulting to explain extension on the northwest side associated with the low-crustal extrusion of the Longmen Shan [e.g., *Jia et al*., 2010]. Others argued that it is a northwest-vergent back thrust associated with the Longmen Shan and Min Shan thrust belts [e.g., *Yin*, 2010]. A preliminary investigation by *Xu et al*. [2008] showed that the Longriba fault zone is dominantly dextral with small southeast-verging thrusting. They also proposed that the Longriba fault zone is a fault newly formed in the late Quaternary. However, its slip rate was poorly constrained. Thus, to fully understand strain partitioning in eastern Tibet, detailed study of slip rates along the Longriba fault zone is necessary.

[4] In addition, the Longriba fault zone consists of two strands: the Longriqu fault in the northwest and the Maoergai fault in the southeast (Figure 2). These two strands are sub-parallel and separated by ~20–30 km. This sub-parallel fault pattern is somewhat similar to the surface rupture of the 2008 Wenchuan earthquake, which ruptured two sub-parallel faults of the Longmen Shan fault zone ~10–15 km

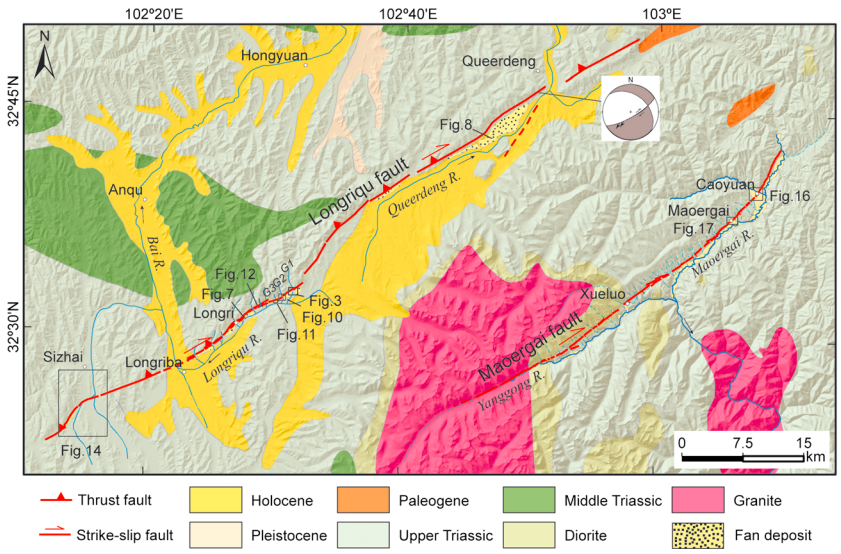

Figure 2. Geologic features and fault distribution of the central Longriba fault zone. See location in Figure 1b. Lithological data are from Geological Bureau of Sichuan Province [1991]. G1, Gailongwa gully; G2, Longergeng gully; G3, Tuokouxia gully. Fault plane mechanism is based on slickenside field data on the fault plane with a strike of 62° and a dip of 75°.

apart [*Ren et al.*, 2010; *Xu et al.*, 2009]: the Yingxiu-Beichuan and Guanxian-Jiangyou faults (Figure 1b), raising the possibility that a large earthquake could rupture both strands of the Longriba fault zone. However, no large historical earthquake is known on this fault [*China Earthquake Administration*, 1999a, 1999b]. Furthermore, due to sparse seismic stations in adjacent areas, only a few small earthquakes have been recorded in this area. Two trenches have been conducted at Caoyuan and Maoergai villages on the Maoergai fault [*Ren et al.*, 2013]. Three events were identified from these trenches. Radiocarbon dating and OxCal model show that these events have a good age correlation in these two sites and occurred at ~8510 ± 420, ~7100 ± 70, and ~5170 ± 80 cal yr B.P., respectively. Based on the seismic displacement estimated from the relation between horizontal offset and apparent vertical displacement on a sloping terrace tread, this fault underwent earthquake with Mw ~7.2. So paleoseismic study on the Longriqu fault is needed to address this question.

[5] Field investigations were conducted in 2010 and 2011. Based on high-resolution satellite imagery and numerical dating, we used trenching to reconstruct the latest Quaternary paleoseismic history of the Longriqu fault and to examine rupture behavior on the two strands of the Longriba fault zone. We also employed displaced terrace risers to determine geological slip rates along the Longriba fault zone and to discuss its role in strain distribution in eastern Tibet. This study is significant to seismic hazard assessment and understanding of kinematic mechanisms in eastern Tibet.

2. Geologic Setting

[6] The eastern margin of the Tibetan Plateau is an active tectonic boundary composed of numerous major northwest-southeast to north-south-striking left-lateral strike-slip faults, such as Kunlun, Xianshuihe, Zemuhe, Xiaojiang, and Litang faults, and some northeast-southwest and north-south-trending thrust faults, such as Longmen Shan, Minjiang, and Lijiang-Xiaojin faults (Figure 1b) [*Yeats et al.*, 1997]. Offset landforms and geodetic measurements have shown that these faults accommodate slip of several to 10 mm/yr due to the eastward extrusion of the Tibetan Plateau and the collision with the rigid Sichuan Basin [*Yeats*, 2012; *Zhang et al.*, 2004]. This region is also seismically active and is known as the middle segment of the China North-south-trending Seismic Zone [*Zhang*, 2013]. Strong earthquakes are primarily concentrated on these faults, suggesting that the sub-blocks bracketed by these faults appear to be rigid [*Cheng et al.*, 2012].

[7] Along the Longmen Shan, structures within the Mesozoic thrust belt formed an imbricate fan of steep, southeast-verging thrust faults that were proposed to merge with a décollement at ~20 km depth beneath the Plateau [*Burchfiel et al.*, 1995; *Hubbard and Shaw*, 2009]. Several of these faults are currently active, including the Yingxiu-Beichuan and Guanxian-Jiangyou faults, the primary structure responsible for the 2008 Wenchuan earthquake. Slip rates on these structures, although not precisely determined, appear to be relatively small (on the order of 1–2 mm/yr) [*Densmore et al.*, 2007; *Zhang et al.*, 2010]. In addition, the range-front fault defining the boundary between the range and basin and several buried fault and folds in the basin have been verified as probably active in the late Quaternary [*Ren et al.*, 2012; *Wang et al.*, 2013].

[8] The Longriba fault zone is a sub-block boundary in the Bayan Har block. Deep seismic reflection profiles across the Longriba fault zone suggested that this fault probably displaced the Moho beneath the Plateau [*Gao et al.*, 2012]. In addition, the fault zone also demonstrates a geomorphic boundary (Figure 1c). To the west, it is the very flat plateau surface, and to the east, it is the high-relief Longmen Shan. Although *Xu et al.* [2008] inferred that the southwest and northeast parts of the Longriba fault zone are also active in late Quaternary, our field observations show that an alluvial terrace formed in late Pleistocene was not displaced by the

faults. The most obvious tectonic geomorphology is along the central part of the Longriba fault zone, suggesting a strong rupture history in the late Quaternary. Thus, our work is focused on this part.

[9] The basement along the central Longriba fault zone involves primarily Triassic igneous rocks including granite and Songpan-Ganzi flysch [*Chen and Wilson*, 1996], consisting of late-Triassic meta-sandstone and slate interbedded with limestone of the Xinduqiao Formation, mid-Triassic slate and phyllite of the Zanaishan Formation (Figure 2). Cenozoic strata consist mainly of Paleogene conglomerate, sandstone and siltstone of the Relu Formation, and Quaternary sediments, including fluvial, alluvial, and eolian deposits [*Geological Bureau of Sichuan Province*, 1991]. Quaternary fluvial and alluvial deposits are composed mainly of sandy gravel, fine sand, silt, and clay, and are primarily distributed along the Maoergai and Bai rivers and their tributaries. The eolian deposits are locally characterized by loess terraces between mountains and river valleys, and thin caps of river terraces. In addition, our study area is located in grassland where there are relatively rich organic layers, enabling the collection of radiocarbon samples within the sediments for dating.

3. Paleoseismology on the Longriqu Fault

[10] The Longriqu fault extends ~85 ± 5 km from south of Sizai Town through Longri Town to Queerdeng Village (Figure 2). In the northeast, it runs primarily along the hillside north of Queerdeng River and is characterized by shutter ridges and linear features. The slickensides on the fault plane south of Queerdeng Village indicate that the Longriqu fault also has a component of a southeast-verging thrusting (Figure 2). In the southwest, the fault cuts through the mountain-front alluvial fans north of Longriqu River, marked by distinctive fault scarps and offset terraces, demonstrating that the fault is right-lateral strike slip with a thrust component dipping northwest. In the southernmost part of the fault, fault scarps and shutter ridges were found south of Sizhai Town (Figure 2). Mountain-front alluvial fans formed on the southeastern side of the fault trace, showing Quaternary uplift on the northwestern side of the fault. Collectively, the above evidence indicates that the Longriqu fault experiences an oblique motion with dominantly dextral slip and a small southeast-verging thrust component.

[11] Southwest of Longri Town, the fault includes two or three strands characterized by fault scarps on mountain-front fans (Figure 2), showing a complex fault system. Northeast of Longri Town, prominent fault scarps on the mountain-front alluvial fans and offset terraces indicate that the displacement is concentrated on one fault. Several gullies cut through the mountain-front fan and flow into the Longriqu River (Figure 2). Three alluvial terraces are generally developed along the gullies. The oldest terrace (T3) from the frontal gullies consists of the frontal alluvial fan deposits and has a similar height above the water level of the Longriqu River, suggesting that terrace T3 and the frontal fan formed coevally. Fault scarps are observed on terraces T3 and T2 but not on the youngest terrace (T1), probably indicating that the fault was not active at the time of terrace T1 formation. According to preliminary dating of river terraces in this region [*Xu et al*., 2008], terrace T3 formed in the late Pleistocene, and terraces T2 and T1 were developed in the Holocene. We excavated a trench across the fault scarp on terrace T3 and found some natural fault exposures with evidence for late Quaternary paleoearthquakes.

[12] Among the various indicators for paleoseismology in unconsolidated sediments within a strike-slip fault setting, the best and clearest indicators for faulting are fault scarps, scarp-derived colluvium, upward termination of faults, offset sedimentary layers, and liquefaction [*McCalpin*, 2009]. In this paper, we use these indicators to identify paleoseismic events.

[13] In order to bracket the age range of event horizons, we collected samples from the bottom of overlying layers and the top of underlying layers. The radiocarbon samples consist of small pieces of charcoal and organic materials originating as grass roots that grew in situ. Therefore, the radiocarbon ages of these samples should roughly represent the time of deposition of the sedimentary units.

3.1. Gailongwa Trench (32°32′46.4″N, 102°31′24.7″E)

[14] Northeast of Longri Town, three fill terraces formed on the southeast bank of Gailongwa Gully (Figure 3). WorldView satellite image with 0.6 m resolution indicates that the fault is characterized by a linear feature (Figure 3a). Fault scarps on terraces T2 and T3 and offset T3/T2 riser can be obviously identified (Figures 3b and 3d). A trench ~10 m long and ~4 m deep was excavated across the fault scarp on the T3 terrace (Figures 4 and 5). The excavation was conducted on the slope of the fault scarp from the site ~1 m below the T3 surface of the hanging wall because the alluvial gravel of T3 of the upper part of the scarp slope is well exposed and no fault is identified. In addition, the sediment in this area has a high water content; marshes on the terraces and terrace risers resulted in large amounts of water accumulating in the trench when we tried to dig deeper on the footwall.

[15] The strata exposed on the south and north walls in the trench are similar and are all unconsolidated; they mainly comprise latest Pleistocene alluvial gravel of T3, latest Pleistocene to Holocene slope wash, and Holocene soil. Eight units are identified from the surface to the bottom on the basis of stratigraphic characteristics and radiocarbon ages (Figure 4c and Table 1).

[16] Unit 1 is alluvial gravel including lower gray alluvial sand with gravel (Unit 1b) and an upper sandy silt (Unit 1a). This unit is apparently more compacted than other units in the trench, suggesting that Unit 1 is the oldest and may be the middle portion of alluvial gravel of terrace T3. Unit 2, consisting of alluvial gravel of terrace T3 in the hanging wall, includes grayish-yellow gravel (Unit 2a) and interbedded clay (Unit 2b). Unit 3 is an alluvial sequence including four parts: brown subangular, poorly sorted gravel with horizontal bedding in the bottom (Unit 3d), gray coarse sand with gravel in the lower part (Unit 3c), blue-gray sandy silt with a thickness of 10–20 cm in the middle part (Unit 3b), and gray-yellow overbank-facies fine sand and sandy silt in the upper part (Unit 3a). Unit 4 represents a sedimentary sequence from colluvium to slope wash on the alluvial sediment. The colluvium (Unit 4a) is composed primarily of poorly sorted brown gravel filled with sand and sandy silt, and the slope wash (Unit 4b) consists of yellowish-gray sand and gravel. The grain size of clasts decreases from colluvium to slope wash. Unit 5 is also a

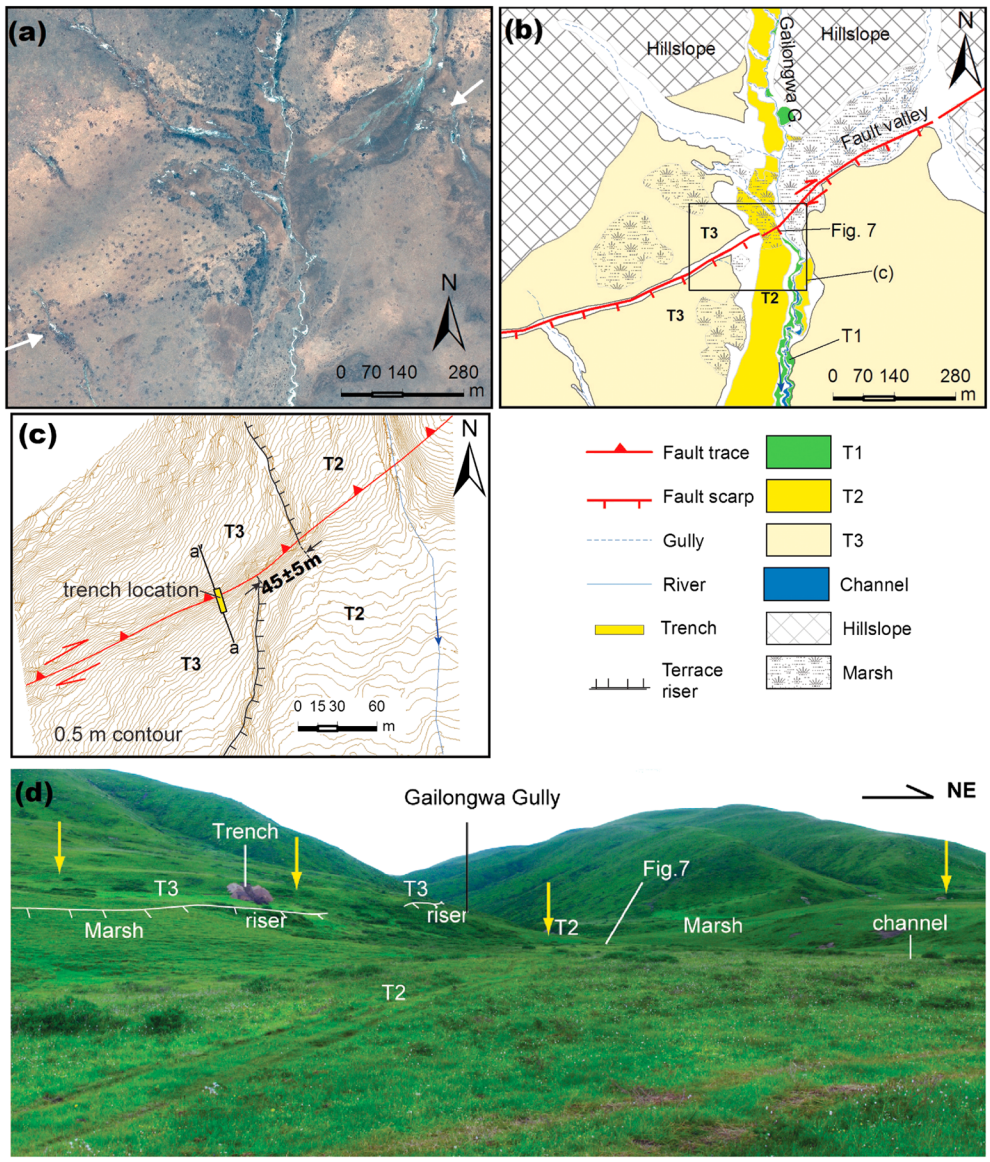

Figure 3. Offset landforms at Gailongwa gully. See location in Figure 2. (a) WorldView satellite image and (b) interpreted map show faulted landforms. White arrows in Figure 3a indicate the location of fault scarps. (c) Topographic survey of offset terraces, conducted by Real Time Kinematic (RTK) GPS with the accuracy of 2 cm horizontally and 5 cm vertically in the field. (d) Photo at the Gailongwa gully, showing fault scarps and offset T3/T2 riser. Arrows show the location of the fault trace.

sedimentary sequence from colluvium (Unit 5c) to slope wash (Units 5a and 5b). The slope wash gravel can be divided into two parts by color: a grayish-black lower part (Unit 5b) and a grayish-yellow upper part (Unit 5a), which are probably related to paleoclimatic fluctuation in the late Quaternary [*Zheng et al.*, 2007]. Unit 6 is a typical slope wash gravel filled with grayish-yellow sandy silt. Unit 7 is a colluvial wedge including a basal colluvial clasts and an overlying slope wash consisting of sand and gravel. The clasts in Unit 7 are more poorly compacted than those in Unit 6, demonstrating that Unit 7 was deposited after Unit 6. Unit 8 is a widespread gray-black soil composed dominantly of decayed grass roots. According to paleoclimate studies in this area [e.g., *Zheng et al.*, 2007], it appears to be related to an interglacial stage since ~4 ka in eastern Tibet.

[17] Although the trench was dominantly alluvial and slope wash clasts, organic materials can be found within clasts. The dating results (Table 1) show that most samples are in stratigraphic order. Two out-of-sequence samples (LRBTC-C-3 and LRBTC-C-4) suggest that the organic sediment samples were probably redeposited as colluvium following erosion of gravel in the hanging wall. This also suggests that the collection of radiocarbon samples should be far from the foot of the colluvium close to the fault. An OSL sample (LRBTC-OSL-8) from Unit 2b is a littler older than radiocarbon age (LRBTC-C-6) (Figure 4c), probably because the alluvial sediments are not completely bleached.

[18] Herein we employ the Bayesian statistical approach to model the age of the units in the Gaimalong trench. In our model, the OxCal radiocarbon calibration and analysis

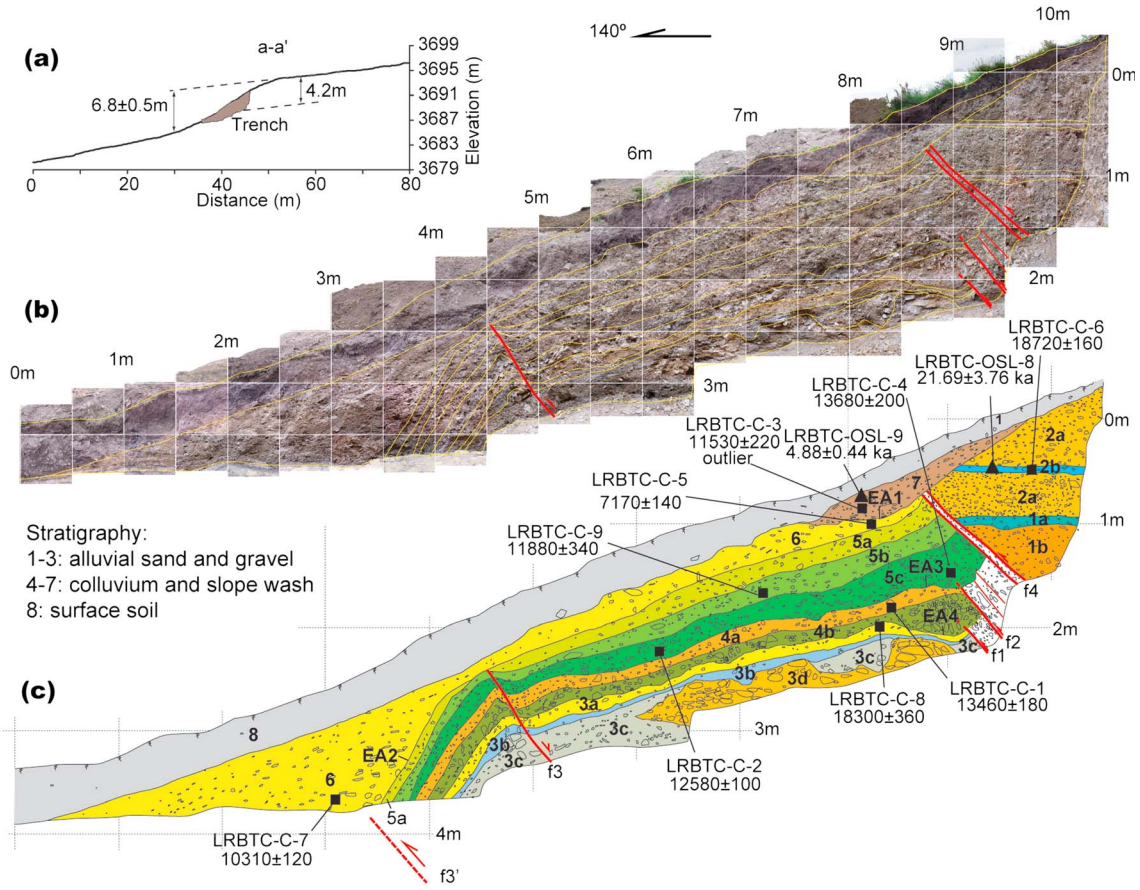

Figure 4. (a) Topographic profile across the fault scarp on terrace T3. See location in Figure 3c. (b) Mosaic photo of the southwest wall of the Gailongwa trench. Red lines show faults. (c) Log of southwest wall of the Gailongwa trench. See trench site in Figures 3c and 3d. Radiocarbon samples are marked by black solid boxes with sample numbers and calibrated ages (cal yr B.P.). OSL samples are shown in black triangles.

software (version 4.1.7) [*Bronk Ramsey*, 2008] based on the IntCal09 calibration curve of *Reimer et al*. [2009] is used. Our OxCal model uses depositional models [simple sequence: *Lienkaemper and Bronk Ramsey*, 2009] that are not depth dependent; namely, the age of undated events are not influenced by burial depth [*DuRoss et al*., 2011].

[19] Based on historical records, no surface-faulting earthquakes have occurred along the Longriba fault, and the earthquake catalog M ≥6 in northern Sichuan was regarded to be complete since 1879 [*Huang et al*., 1994]. Then this date is a historical upper bound in our model. The Boundary command was used at the beginning of the sequence for this model.

[20] The Phase command was used to describe stratigraphic units including several radiocarbon ages from the R_Date command, as illustrated by *Lienkaemper and Bronk Ramsey* [2009]. The Boundary command paired with a separate Zero_Boundary command is introduced to illustrate the condition when the event is closer to one of two ages, as proposed by *DuRoss et al*. [2011]. Calibrated dating results of samples and events by the OxCal model are expressed as the mean with two-sigma (2σ; 95%) uncertainty (Table 1).

[21] The major fault zone is a ~1 m wide shear zone including three faults (f1, f2, and f4) mainly focused at meter ~9 in the trench, characterized by displaced layers and oriented clasts (Figure 4c) showing that the faults underwent reverse displacement. Another fault (f3) located at meter ~5 deformed Units 3–5, showing a normal separation. Based on stratigraphic characteristics and contact relationships in the trench, we identify four surface-faulting events (named EA1-EA4 from young to old).

[22] The earliest event (EA4) displaced the top of alluvial deposits of terrace T3 (Unit 3a) along fault f1 (Figure 4c) and generated a scarp on the terrace surface (Figure 6b). Subsequent colluvial gravel and slope wash (Unit 4a) covered fault f1 (Figure 6c). So EA4 postdates Unit 3a and predates Unit 4a. A radiocarbon sample (LRBTC-C-8) taken from the upper part of Unit 3a shows that the T3 terrace was abandoned at ~18,300 cal yr B.P., and another sample (LRBTC-C-1) collected from the middle part of the slope wash (Unit 4a) overlying the colluvium suggests that EA4 predated ~13,460 cal yr B.P. (Figure 4). The OxCal model shows that the earliest event (EA4) occurred at 17,830 ± 530 cal yr B.P. (Figure 5).

[23] The next event (EA3) occurred along fault f2 (Figure 4c). It offset Unit 4 and produced a scarp on the top of Unit 4a (Figure 6d). Subsequently, the colluvium and slope wash (Unit 5) were deposited on Unit 4 (Figure 6e). Thus, EA3 postdates Unit 4a and predates Unit 5. Unit 5 is apparently thicker than Unit 4 (Figure 4c), suggesting a higher fault scarp related to EA3. In addition, sample LRBTC-C-4 collected from the bottom of the colluvial clasts (Unit 5c) yields an age of 13,680 ± 200 cal yr B.P., similar to Unit 4a

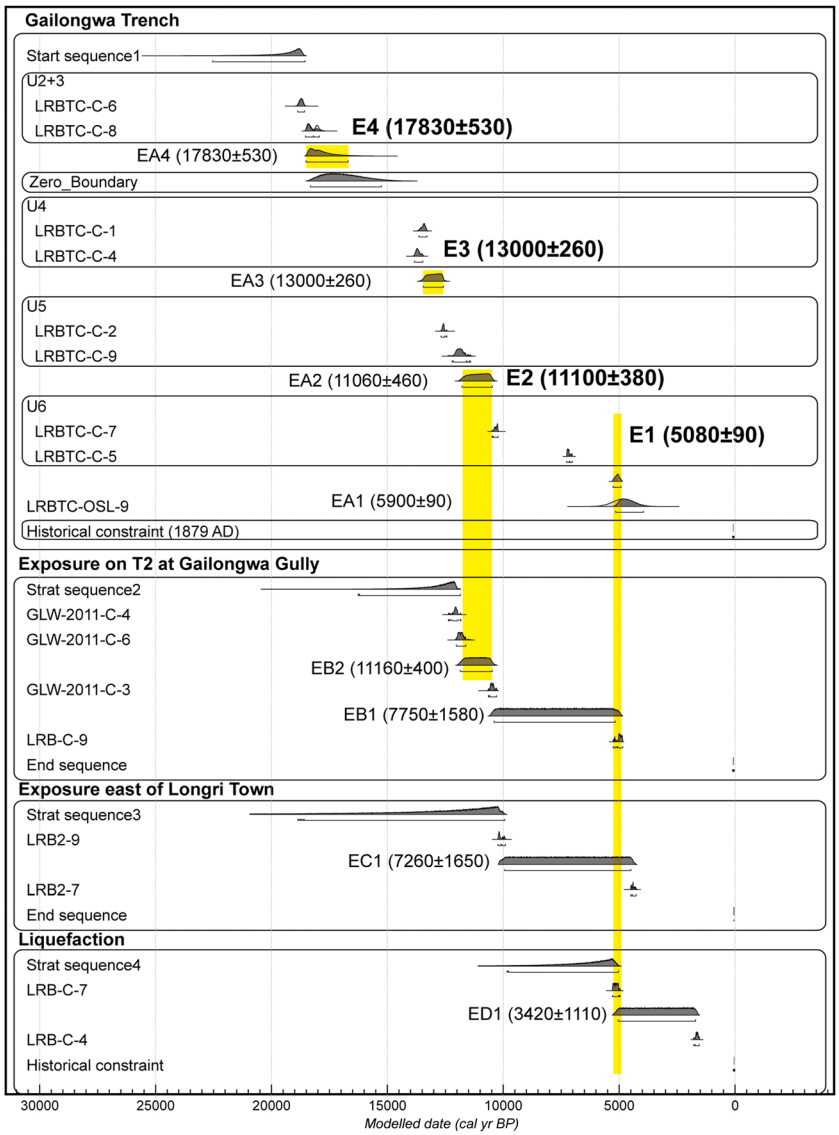

Figure 5. Results of the OxCal analysis of radiocarbon dates along the Longriqu fault. Open curves represent the prior probability distribution. Filled curves represent the posterior distributions. Calibrated dates are presented with 2σ age range (95% density). Dating results of samples are shown in Table 1. See text for detailed explanation.

(Figure 4c), probably implying that the sample accumulated with colluvium after it had been deposited in the slope wash following EA4. A radiocarbon sample (LRBTC-C-2) collected from the slope wash of Unit 5 yields an age of 12,580 ± 100 cal yr B.P. The OxCal model shows that EA3 occurred at 13,000 ± 260 cal yr B.P. (Figure 5).

[24] The penultimate event (EA2) ruptured fault f3 (Figure 4c). This event deformed and tilted a series of distinctive layers in color and grain size with a vertical displacement of ~20 cm (Units 3–5), representing a small normal fault dipping northwest. We propose that the main fault (f3′) related to EA2 is a reverse fault at the foot of the tilted layers (Figure 4c). Fault f3 is probably a secondary fault accompanying fault f3′ (Figures 6f and 6g). Following EA2, a thick slope wash (Unit 6) formed at the scarp (Figure 6g). Due to large amounts of water from the bottom of the trench, the northeast wall of the trench collapsed and the top of alluvial gravel in the footwall could not be reached. Based on stratigraphic relations, we infer that EA2 occurred after Unit 5 and prior to Unit 6. A radiocarbon sample (LRBTC-C-9) from Unit 5b yields an age of 11,880 ± 200 cal yr B.P., and an organic sediment sample (LRBTC-C-7) taken from the middle part of slope wash (Unit 6) yields an age of 10,310 ± 120 cal yr B.P. (Figure 4c). The Oxcal model constrains the age of EA2 to 11,060 ± 460 cal yr B.P. (Figure 5).

[25] The last event (EA1) is demonstrated by the colluvial wedge (Unit 7) (Figure 4c). It underwent displacement along fault f4 and dislocated Unit 6. Fault f2 and some small faults in the major shear zone might be reactivated to deform the bottom of Unit 5c (Figure 4c). A scarp formed at fault f1 following EA1, and subsequently, the colluvial wedge was deposited (Figures 6h and 6i). Thus, EA1 postdates the slope wash of the colluvial wedge (Unit 6) related to event EA2 and predates Unit 7. An OSL sample (LRBTC-OSL-9) taken

Table 1. Radiocarbon Dating Results[a]

Sample No.	Beta No.	Material	Tech.[b]	^{14}C Age (Mean ± σ/B.P.)	Calibrated Age[c] (cal yr B.P.)
			Gailongwa trench		
LRBTC-C-1	306273	Organic sediment	AMS	11,600 ± 60	13,460 ± 180
LRBTC-C-2	311814	Organic sediment	AMS	10,640 ± 50	12,580 ± 100
LRBTC-C-3	306274	Organic sediment	AMS	10,030 ± 40	11,530 ± 220
LRBTC-C-4	306275	Organic sediment	AMS	11,840 ± 60	13,680 ± 200
LRBTC-C-5	306276	Organic sediment	AMS	6250 ± 40	7170 ± 140
LRBTC-C-6	306277	Organic sediment	AMS	15,530 ± 70	18,720 ± 160
LRBTC-C-7	306278	Organic sediment	AMS	9140 ± 50	10,310 ± 120
LRBTC-C-8	306279	Organic sediment	AMS	14,890 ± 60	18,300 ± 360
LRBTC-C-9	311815	Organic sediment	AMS	10,190 ± 80	11,880 ± 340
			Natural exposure at terrace T2 of the Gailongwa gully		
GLW-2011-C-3	306269	Charcoal	AMS	9300 ± 50	10,480 ± 160
GLW-2011-C-4	311813	Charcoal	AMS	10,290 ± 40	12,080 ± 180
GLW-2011-C-6	306289	Organic sediment	AMS	10,160 ± 50	11,840 ± 220
LRB-C-9	289925	Charcoal	AMS	4410 ± 40	5020 ± 220
			Liquefaction south of Queerdeng Village		
LRB-C-4	288500	Organic sediment	AMS	1760 ± 40	1670 ± 120
LRB-C-7	288502	Charcoal	AMS	4500 ± 40	5160 ± 160
			Natural exposure east of Longri Town		
LRB2-7	-	Charcoal	AMS	3955 ± 35	4410 ± 140
LRB2-9	-	Charcoal	LSC	8985 ± 50	10,120 ± 200
			Site of Longergeng gully		
LEG-2011-C-1	306270	Charcoal	AMS	640 ± 30	610 ± 60
LEG-2011-C-2	306271	Charcoal	AMS	2050 ± 30	2020 ± 100
			Site of Tuokouxia gully		
LEGW-2011-C-1	306272	Charcoal	AMS	6330 ± 40	7260 ± 100
			South of Sizhai Village		
ZL-2011-C-1	306286	Charcoal	AMS	9260 ± 50	10,430 ± 160

[a]Samples with the prefix "LRB2" are from *Xu et al*. [2008]. Our samples were analyzed by Beta Analytic Inc.
[b]AMS, accelerator mass spectrometry; LSC, Liquid Scintillation Counting.
[c]Calendar ages calibrated using OxCal 4.1 based on IntCal 09 curve [*Reimer et al*., 2009]. Associated age range reported at 2σ.

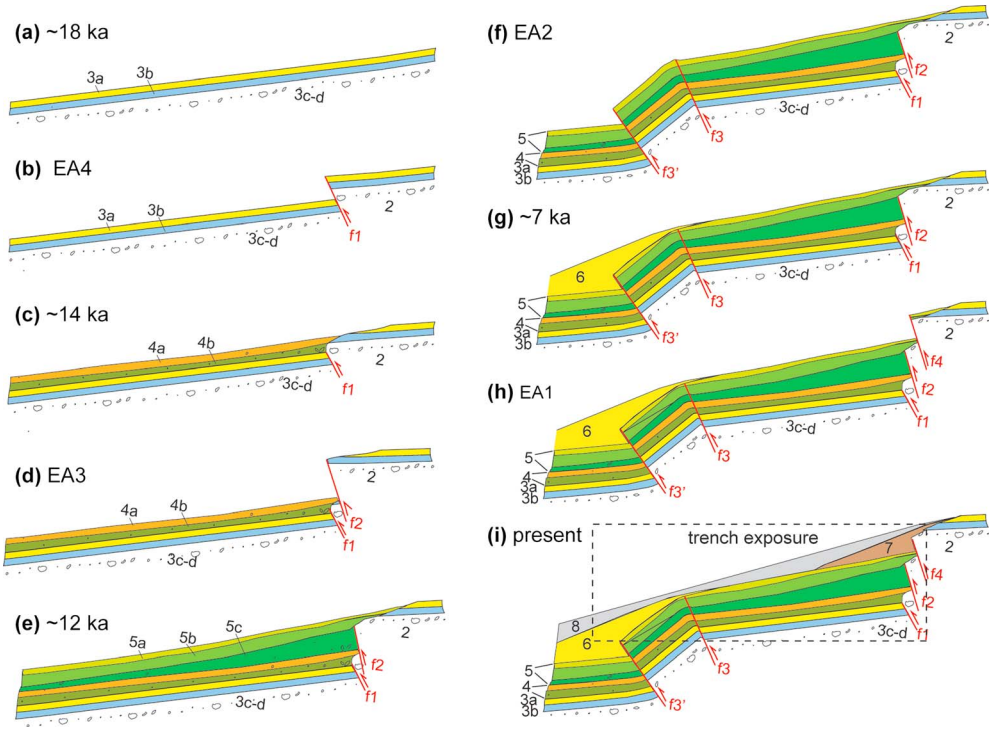

Figure 6. Restoration of Gailongwa trench showing faulting and deposition at the trench site. (a)–(i) The oldest to present process. Strata thicknesses are not strictly based on the actual values. Unit colors and labels are same as shown in Figure 4c.

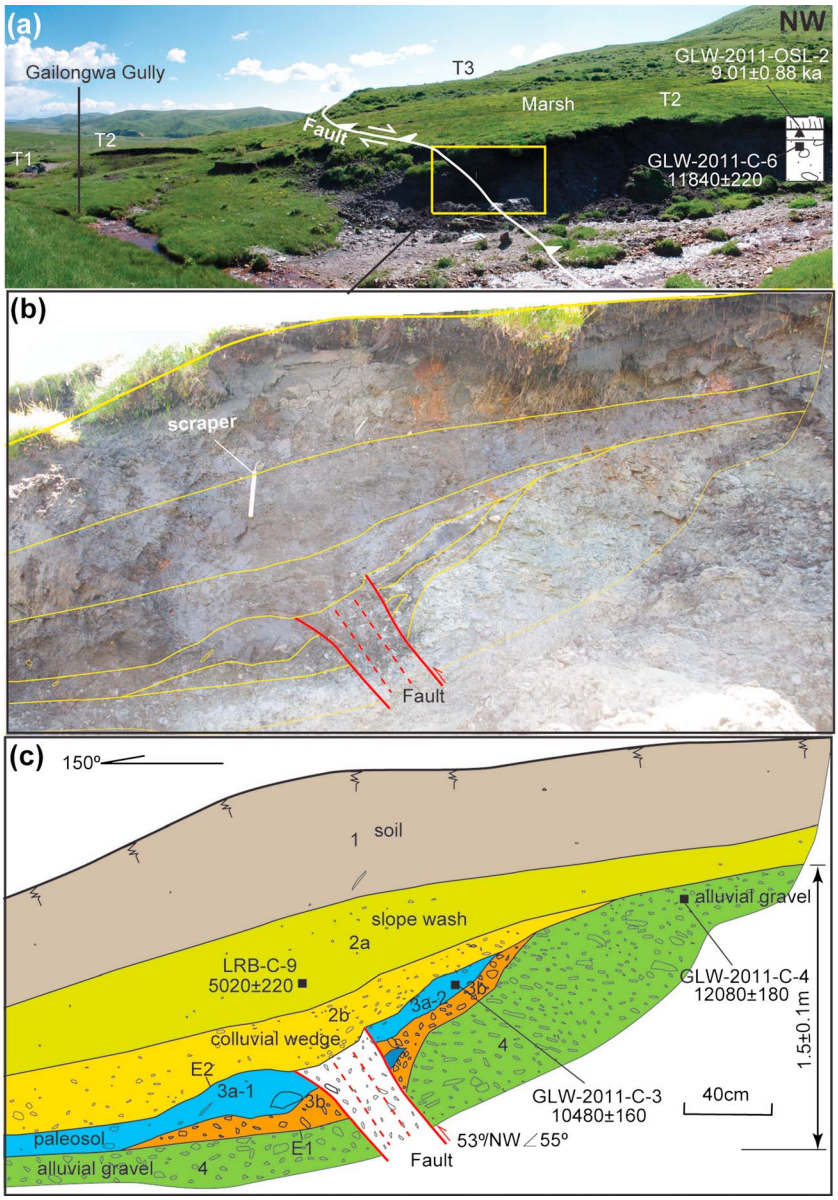

Figure 7. Fault exposure in terrace T2 of the Gailongwa gully. See location in Figures 3b and 3d. (a) Photo indicating fault scarp on terrace T2. (b) Photo and(c) log of the fault outcrop demonstrate vertical displacement of alluvial gravel of T2, equivalent to the height of fault scarp on terrace T2. Radiocarbon samples are marked by small black solid boxes with sample numbers and calibrated ages (cal yr B.P.). Black triangle shows OSL sample.

from the slope wash of the colluvial wedge of EA1 (Figure 4c) suggests that event EA1 occurred before ~4.8 ka. Our OxCal model yields the EA1 age of 5900 ± 90 cal yr B.P. (Figure 5).

3.2. Natural Exposure in the T2 Terrace of the Gailongwa Gully (32°32′50.7″N, 102°31′29.6″E)

[26] WorldView image and field investigation demonstrate that the fault also displaced terrace T2 in Gailongwa Gully and formed a fault scarp on the terrace surface (Figure 7a). A marsh formed on terrace T2 and across the fault scarp, probably lowering the height of the fault scarp. A natural fault exposure was found on the southwest bank (Figure 7b).

[27] The strata in the section can be divided into four units (Figure 7c). Unit 1 is a present-day marsh deposit covered on terrace T2 and marked by black turf consisting of decayed and living grass roots. This unit is saturated with water. Unit 2 includes two parts. The upper part (Unit 2a) is a gray-black silt clay with slope wash clasts including abundant decayed grass roots, probably suggestive of a paleo-turf representing a paleo-surface. The lower part (Unit 2b) is a gray-brown poorly sorted gravel layer mixed with sandy silt, representing a scarp-derived colluvium. Thus, Unit 2 represents a colluvial wedge. Unit 3 is another colluvial wedge and consists of lower colluvial gray-brown gravel with blackish sandy silt (Unit 3b) and upper gray-black sandy silt

(Unit 3a) probably representing another paleo-surface. Unit 4 is alluvial gravel of terrace T2.

[28] The fault is marked by a ~30 cm wide shear zone consisting of oriented clasts (Figures7b and 7c). The offset of the top of alluvial gravel of T2 is ~1.5 m (Figure 7c), indicating a reverse displacement on terrace T2. The fault offset Unit 3 and produced a small scarp but is overlain by unfaulted colluvium (Unit 2).

[29] We identify two events from this natural exposure. The penultimate event (EB2) ruptured Unit 4 and produced a scarp on terrace T2. Subsequently, the colluvial wedge (Unit 3) accumulated at the scarp. A paleo-surface was formed on the colluvial wedge. So EB2 postdates Unit 4 and predates Unit 3. A charcoal sample (GLW-2011-C-4) taken from the top of alluvial gravel (Unit 4) yields an age of 12,080 ± 180 cal yr B.P. (Figure 7c), consistent with another organic sediment sample collected from an organic sediment lens in the upper alluvial gravel and the OSL sample (GLW-2011-OSL-6) from the overlying sandy silt capping alluvial gravel of T2 ~6 m north of the natural exposure (Figure 7a). These dating results reveal an abandonment age of ~12 ka for the T2 gravel. A charcoal sample (GLW-2011-C-3) from the paleosol (Unit 3a) yields an age of 10,480 ± 160 cal yr B.P. (Figure 7c). The OxCal model shows that EB2 occurred at 11,160 ± 400 cal yr B.P. (Figure 5).

[30] The last event (EB1) dislocated Unit 3, and the subsequent colluvial gravel (Unit 2b) and the turf layer (Unit 1) were deposited (Figure 7c). A small scarp on the top of Unit 3 suggests that EB1 has a smaller vertical displacement than EB2, consistent with the result of Gailongwa trench. EB1 may undergo a dominantly strike-slip motion. Thus, EB1 occurred after Unit 3a and prior to Unit 2. Unit 2 was not deformed, which indicates that EB1 is the last surface-faulting event. A charcoal sample collected from the slope wash (Unit 2a) overlying the colluvium (Unit 2b) yields an age of 5020 ± 200 cal yr B.P. (Figure 7c). Based on the OxCal result, EB1 occurred at 7750 ± 1580 cal yr B.P. (Figure 5).

3.3. Natural Exposure East of Longri Town (32°32′13.5″N, 102°30′05.9″E)

[31] East of Longri Town, a fault exposure was found in a small gully (Figure 7) [*Xu et al*., 2008]. It displaced the lower part of the section and was covered by subsequent sediments. The strata in the section consist of five units (Figure 8). Unit 1, the gray-black humus interbedded with a gravel lens, represents the present soil. Unit 2 is the slope wash gravel. Unit 3 is a gray-yellow gravel interbedded with sandy silt. The grayish-black upper part of Unit 3 implies that it has been pedogenically altered and represents a paleo-surface. Unit 4 is composed primarily of gray sandy silt, likely representing an overbank facies. Unit 5 consists of gray or grayish-yellow alluvial gravel.

[32] From the section, only one surface-faulting event (EC1) can be identified. The fault displaced Units 4 and 5 and produced a fault scarp (Figure 8). The sediments derived from the scarp (Units 2 and 3) were deposited following event EC1. Thus, EC1 postdates Unit 4 and predates Unit 3. A charcoal sample (LRB2-7) taken from Unit 4 yields an age of 10120 ± 200 cal yr B.P., and another charcoal sample (LRB2-9) from the top of Unit 3 yields an age of 4410 ± 140 cal yr B.P. (Figure 8). Our OxCal model shows

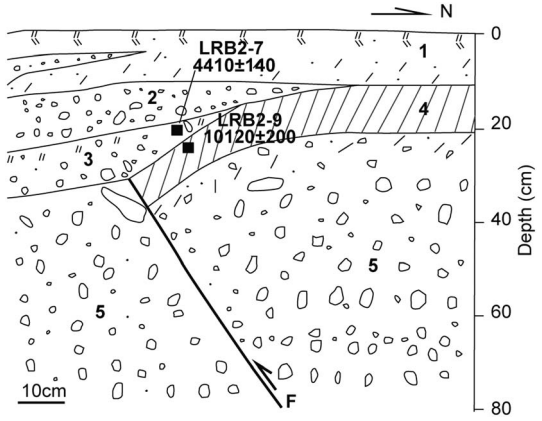

Figure 8. Fault exposure in an alluvial terrace northeast of Longri Town, modified after *Xu et al*. [2008]. See location in Figure 2. Radiocarbon samples are marked by small black solid boxes with sample numbers and calibrated ages (cal yr B.P.). The lack of Unit 4 in the footwall suggests a local deposit that was offset by the dominantly strike-slip fault.

that EC1 occurred at 7260 ± 1650 cal yr B.P. (Figure 5). The absence of Unit 4 on the footwall suggests that Unit 4 was locally deposited and offset by strike-slip faulting.

3.4. Liquefaction South of Queerdeng Village (32°43′35.5″N, 102°46′50.5″E)

[33] As mentioned above, because the northeast segment of the fault extends along the hillside, it is hard to find a section showing that the fault dislocated Quaternary sediments. In the mountain-front alluvial fan south of Queerdeng Village, a sand blow was found in the alluvial deposits (Figure 9).

[34] The strata in this section are composed of four parts (Figure 9). Unit 1 is the present-day gray soil filled with some gravel and large amounts of grass roots. Unit 2 is alluvial gravel including an upper sand and gravel (Unit 2a) and a lower gravel (Unit 2b). Unit 3 is overbank-facies brown silt clay with an interlayer of marsh gray silt containing charcoal. Unit 4 is composed primarily of coarse sand filled with fine gravel.

[35] The section indicates that the coarse sand in Unit 4 penetrated Unit 3 and was ejected onto the surface of Unit 3 to form a sand blow (Figure 9). At this site, the alluvial fan is flat and nearby hillsides are low relief. The paucity of the conditions for landslides suggests that this liquefaction is associated with strong seismic shaking. Subsequently, the sand blow was covered by alluvial gravel of Unit 2. Thus, this paleoearthquake occurred after the formation of Unit 3 and prior to Unit 2. A charcoal sample (LRB-C-7) from the marsh interlayer in Unit 3 yields an age of 5160 ± 160 cal yr B.P., and an organic sediment sample (LRB-C-4) from the upper part of Unit 2b yields an age of 1670 ± 120 cal yr B.P. (Figure 9 and Table 1). Our OxCal model shows that this event (ED1) occurred at 3420 ± 1110 cal yr B.P. (Figure 5).

[36] Except for the Longriba fault zone, the nearest active fault is the Minjian fault >150 km away (Figure 1b). So, this paleo-liquefaction is interpreted to be the result of activity on the Longriba fault zone. The Maoergai fault is ~25 km away and is separated from the liquefaction site by mountains

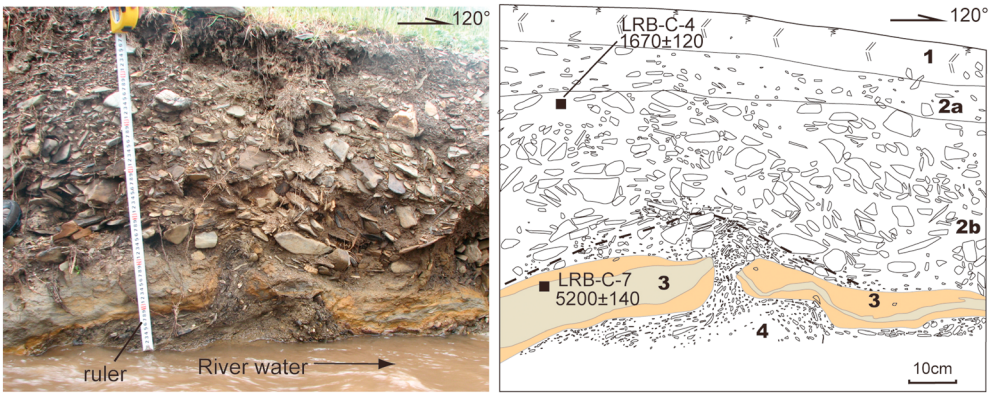

Figure 9. Sand blow in the alluvial fan at the eastern segment of the Longriba fault, south of Queerdeng Village. See location in Figure 2. The dashed line shows the possible top of sand blow based on the injected coarse sand and fine gravel from Unit 4.

(Figure 2). It allows for a maximum earthquake of Mw ~7.2 based on the length of the Maoergai fault (~65 km) using the regression relationship of length of fault rupture and magnitude from *Wells and Coppersmith* [1994]. In addition, the liquefaction site does not lie in the rupture propagation direction of the Maoergai fault. Thus, we infer that the seismic liquefaction is probably related to the Longriqu fault.

3.5. Summary

[37] The foregoing indicates that four paleoearthquakes have occurred on the Longriqu fault in the late Quaternary. Their ages are well constrained by radiocarbon and OSL samples from the overlying and underlying layers. At a first approximation, the last two events demonstrate a good age correlation at the four sites. So we construct a new OxCal model to determine the age of these events along the Longriqu fault. The "=" notation is introduced to illustrate that an event also ruptured other sites. The model demonstrates that the four events (E1–E4) occurred at 5080 ± 90; $11{,}100 \pm 380$; $13{,}000 \pm 260$; and $17{,}830 \pm 530$ cal yr B.P., respectively (Figure 5). Notably, the last event occurred ~5000 years ago. The earlier two events (E3 and E4) are only discovered in the Gailongwa site, and their age are determined according to the dating results of the Gailongwa trench.

[38] According to the empirical relationship proposed by *McCalpin* [2009], the vertical displacement associated with one event is approximately twice the maximum thickness of the fault-derived colluvial wedge associated with it. Reverse faults typically form scarps steeper than the angle of repose of faulted materials. This type of scarps may generate scarp-derived colluvium, deposited by gravity, debris, and wash processes, in a manner similar to that described for normal faults [*McCalpin*, 2009]. This relationship is based on direct observations made on fault ruptures and the fact that the coseismic colluvial wedges are made of clasts derived from the rapid degradation of the scarp after the faulting so that their maximum thickness is approximately half of the original scarp height before its collapse. A recent trenching study in the compressional environment also suggested that this relation can provide a minimum estimate of vertical displacement [*Ortuño et al.*, 2012]. In the Gailongwa site, the fault dips ~50°and offsets the unconsolidated alluvial sediments of terrace T3. Therefore, the empirical relationship is probably applicable to the Gailongwa trench.

[39] It is noted that the colluvial wedge herein is composed of composed of colluvium in the lower part and slope wash in the upper part. The thickness is measured from the bottom of the colluvial wedge to the intersection of the top of the slope wash and the fault. In order to remove the effect of near-fault deformation, the intersection was determined by the trend line of the top of slope wash in the trench log. The uncertainty of the colluvial-wedge thickness is estimated from different determinations of the bottom and top of the colluvial wedge. In the Gaimalong trench, the thicknesses of colluvial wedges related to E1, E3, and E4 were measured to be $\sim 0.5 \pm 0.1$, $\sim 0.8 \pm 0.2$, and $\sim 0.5 \pm 0.1$ m, respectively. These data suggest that the coseismic vertical displacements for E1, E3, and E4 are $\sim 1.0 \pm 0.2$, $\sim 1.6 \pm 0.4$, and $\sim 1.0 \pm 0.2$ m, respectively. Their sum (3.6 ± 0.6 m) is a minimum estimate of vertical displacements, approximately consistent with the vertical offset (~4.2 m) of the alluvial gravel of T3 along faults f1, f2, and f4.

[40] In the process of the excavation, we tried to discover the top of Unit 5 in the footwall of fault f3′. When we reached ~50 cm deeper than the present bottom, influx of water led to the collapse of the trench wall, and some part of the trench was backfilled. The visible scarp height at f3′ in the trench is ~1.5 m, indicating that the vertical displacement of E2 should be bigger than ~2.0 m. From the height (~6.8 m) of the fault scarp and the vertical offset (~4.2 m) of the alluvial gravel of T3 along faults f1, f2, and f4, the estimate of the vertical displacement for E2 is ~2.6 m. In addition, no fault scarp at the foot of the scarp or deformation of Unit 6 was found (Figure 4a). Thus, we infer that E2 ruptured faults f3 and f3′ and had a vertical displacement of ~2.6 m. This event with the higher fault scarp may be attributed to a larger earthquake.

[41] In summary, the sum of the vertical displacements of these four events is roughly equivalent to the height of the fault scarp, implying that the paleoseismic history in the Gailongwa trench is probably complete.

4. Slip Rates Along the Longriba Fault Zone

[42] Field investigations show that the Longriqu fault experiences an oblique movement with dominant right-lateral

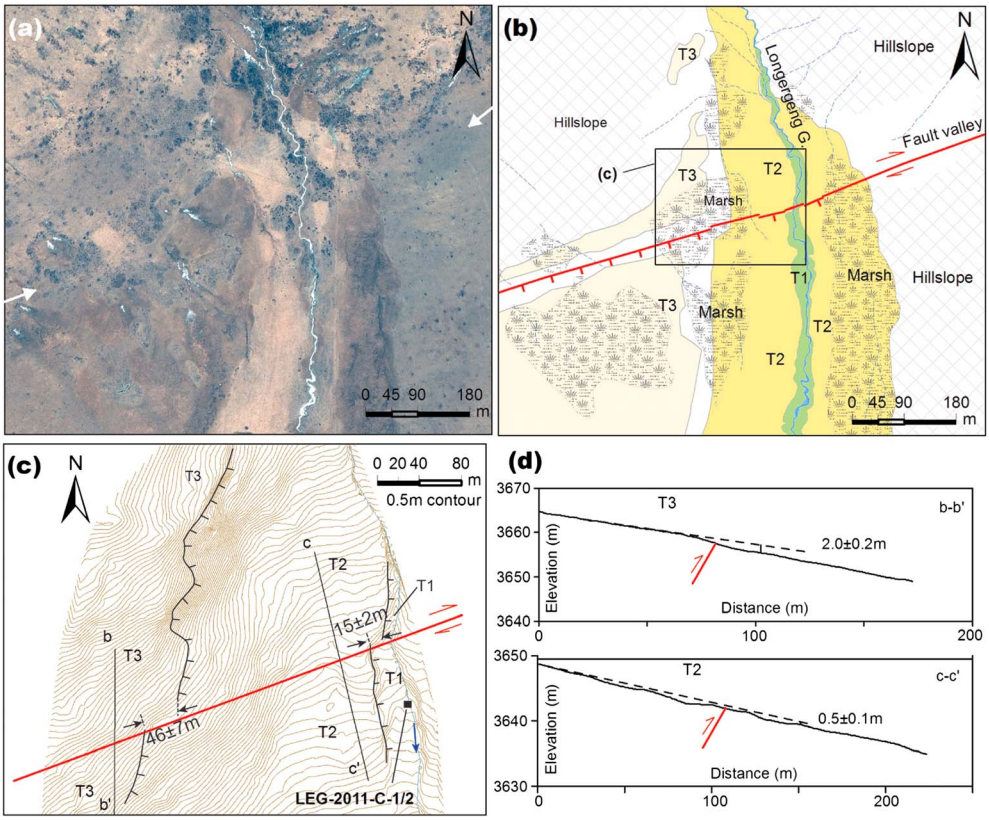

Figure 10. Faulted landforms at Longergeng gully. See location in Figure 2. (a) WorldView image and (b) geomorphic interpretation shows faulted terraces. White arrows in Figure 10a show the location of fault scarps. See legend in Figure 3. (c) Topographic survey of faulted landforms showing fault scarps and offset T3/T2 and T2/T1 risers. (d) Topographic profiles on T3 and T2 located in Figure 10c.

slip and dip-slip component, whereas the Maoergai fault is a pure right-lateral motion. The faults cut through numerous drainages, providing a good opportunity to determine fault slip rates.

[43] The vertical slip rate can be directly estimated by the ratio of the vertical displacement on the terrace and the terrace age. The horizontal rate generally depends on an offset riser between the upper and lower terraces. The horizontal displacement can be obtained by means of a detailed topographic survey. We did not use the intersection of the base of the risers with the lower treads because the loess and colluvial materials obscure these contacts, if the riser crest is well preserved. *Gold et al*. [2011] proposed an approach that considers two projections for each riser crest on the fault to estimate minimum and maximum offsets: one based on the trend of the riser nearest the fault and a second based on the average trend for the entire length of the riser. We use this approach in this study. The reported offset is the mean value between the minimum and maximum offsets, with an uncertainty that is one half this range.

[44] In estimating horizontal slip rates, a debate is ongoing about the age of which terrace that can be assigned to the offset riser [e.g., *Cowgill*, 2007; *Kirby et al*., 2007; *Zhang et al*., 2007]. Our paleoseismic work on the Maoergai fault indicates that the sum of the coseismic horizontal slip of three events identified from the trench on terrace T2 is remarkably equivalent to the offset of the T2/T1 riser [*Ren et al*., 2013], demonstrating that the upper terrace is probably responsible for the offset riser. This conclusion is in good agreement with the model for settings where the stream has insufficient lateral erosion capabilities to remove lateral riser offset [*Cowgill*, 2007; *Lensen*, 1968; *Mason et al*., 2006; *Mériaux et al*., 2005]. Considering that the offset streams along the Longriqu and Maoergai faults have limited flux, we, therefore, use the age of the upper terrace to calculate horizontal slip rates in this paper.

[45] Because age and displacements are uncertain, slip rate estimates derived from them are also uncertain. How to properly calculate slip rate and corresponding uncertainties is a subject of debate. Recently, *Zechar and Frankel* [2009] proposed a new approach to deal with this problem. In this approach, estimates of age, offset, and slip rate at each study site are treated and reported in terms of probability distributions (boxcar, gaussian, trapezoid, and arbitrary) rather than simply as scalar quantities. The slip rate distribution is calculated by convolution based on the probability distributions for age and offset. Age, offset, and slip rate estimates are reported as a median value with upper and lower confidence bound limits. *Zechar and Frankel* [2009] and *Fletcher et al*. [2011] applied this approach to several faults and obtained well-constrained slip rates. Here, we also estimate the slip rate of the Longriba fault zone employing this approach and the corresponding Matlab code [*Zechar and Frankel*, 2009].

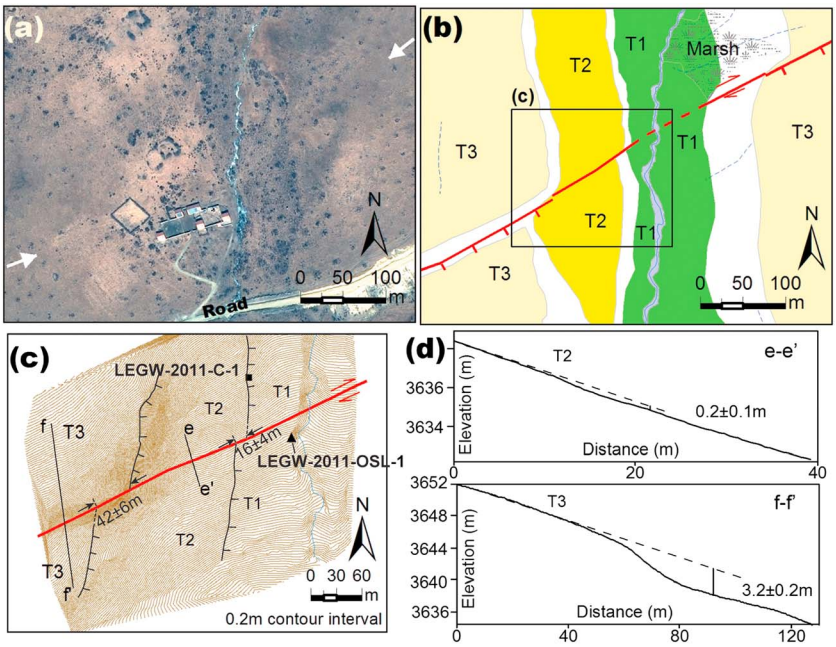

Figure 11. Offset landforms along the Tuokouxia gully. See location in Figure 2. (a) WorldView imagery and (b) geomorphic interpretation shows faulted terraces. See legend in Figure 3. (c) Topographic survey of faulted landforms showing fault scarps and offset T3/T2 and T2/T1 risers. (d) Topographic profiles on T3 and T2. See their locations in Figure 11c.

4.1. Longriqu Fault

[46] As mentioned above, the northeast segment of the Longriqu fault runs through the hillside, whereas its southwest segment cut though alluvial fan and displaced gullies. Northeast of Longri Town, three gullies from the northwestern hillside flow into Longriqu River and have a similar-sized drainage, suggesting that they share the same erosion base level (riverbed of Longriqu River). The Longriqu fault offset these three gullies and produced fault scarps and displaced terrace risers (Figure 2).

4.1.1. Site of Gailongwa Gully

[47] From section 3.1, three terraces (T3–T1) are developed along the Gailongwa valley (Figure 3). Terrace T3 is ~14 m high above the present valley. Terraces T2 and T1 are ~2 m and ~1 m high above the present valley, respectively. Topographic survey indicates that the T3/T2 riser was dextrally offset by ~45 ± 5 m (Figure 3c). The fault scarp on T3 is 6.8 ± 0.5 m high (Figure 4a). Terrace T3 formed at ~18 ± 0.2 ka according to the sample (LRBTC-C-8) taken from the overbank facies of terraceT3 in the Gailongwa trench (Figure 4c).

[48] Terrace T1 is not preserved along the fault trace so the offset of the T2/T1 riser cannot be obtained. The natural fault exposure on terrace T2 gives a vertical displacement of ~1.5 ± 0.1 m (Figure 7c). Radiocarbon samples collected from the top of alluvial deposits of terrace T2 allow us to confidently conclude that the T2 terrace formed at ~11 ± 0.1 ka (Figure 7).

4.1.2. Site of Longergeng Gully (32°32′32.1″N, 102°30′32.3″E)

[49] In the Longergeng gully, three terraces are also well preserved along the valley (Figure 10). Terrace T3 is ~15 m high above the present valley. Terraces T2 and T1 are ~2.5 m and ~1.5 m high above the present valley, respectively. The fault trace is characterized remarkably by fault scarps on terraces T2 and T3 and offset terrace risers. A charcoal sample (LEG-2011-C-1) collected from the bottom of the overlying soil layer of terrace T1 yields an age of 610 ± 30 cal yr B.P.; another charcoal sample (LEG-2011-C-1) taken from the upper alluvial sediments of T1 yields an age of 2020 ± 50 cal yr B.P. (Figure 10c and Table 1). These two dates indicate that the T1 terrace formed ~2 ka. Field observations show that no fault scarp is found on terrace T1, indicating that terrace T1 was not displaced, consistent with the paleoseismic result. On the east bank, the fault cuts through the low-relief hillside and is expressed by a fault valley.

[50] Detailed topographic measurement shows that the right-lateral offset of the T3/T2 and T2/T1 risers are 46 ± 7 and 15 ± 2 m, respectively (Figure 10c). The fault scarp on terrace T3 is 2.0 ± 0.2 m high, and the vertical displacement on terrace T2 is only 0.5 ± 0.1 m (Figure 10d).

4.1.3. Site of Tuokouxia Gully (32°32′14.3″N, 102°29′58.5″E)

[51] In the Tuokouxia gully, three terraces are also well developed on the west bank (Figure 11). Terrace T3 is ~13 m high above the present valley. Terraces T2 and T1 are ~3 m and ~1 m high above the present valley, respectively. The fault is marked by a fault scarp on T3 and offset terrace risers. There is no fault scarp on terrace T1, whereas the vertical deformation on terrace T2 was characterized by a flexure. Topographic surveys indicate that the height of the fault scarp on T3 is 3.2 ± 0.2 m, whereas the vertical deformation on terrace T2 is very small (0.2 ± 0.1 m) (Figure 11d). The riser between terraces T3 and T2 was dextrally offset 42 ± 6 m, whereas the T2/T1 riser was horizontally faulted 16 ± 4 m (Figure 11c). An OSL sample (LEGW-2011-OSL-1) gathered from the bottom of sandy

Table 2. OSL Age Results[a]

Lab No.	Sample No.	Tech.	Dose Rate (Gy/ka)	De (Gy)	Age (ka)
12-OSL-81	LRBTC-OSL-8	SAR	5.41 ± 0.47	117.39 ± 18.08	21.69 ± 3.76
12-OSL-82	LRBTC-OSL-9	SAR	4.85 ± 0.41	23.66 ± 0.99	4.88 ± 0.44
12-OSL-76	LEGW-2011-OSL-1	SAR	5.10 ± 0.47	7.43 ± 0.45	1.46 ± 0.15
12-OSL-78	LEGWW-2011-OSL-1	SAR	5.42 ± 0.48	75.48 ± 9.87	13.94 ± 2.14
12-OSL-79	LEGWW-2011-OSL-2	SAR	5.48 ± 0.50	41.89 ± 3.70	7.65 ± 0.91
12-OSL-73	GLW-2011-OSL-2	SAR	4.97 ± 0.44	47.63 ± 4.37	9.59 ± 1.17
-	LRB2-TL2	SMAR	4.1 ± 0.4	63.2 ± 2.3	15.5 ± 1.7
-	LRB2-TL2	SMAR	3.9 ± 0.4	43.6 ± 1.3	15.5 ± 1.7
-	MEG-TL3	SMAR	4.1 ± 0.4	82.3 ± 3.1	20.7 ± 2.2

[a]Samples without lab no. are from *Xu et al*. [2008]. SAR, single aliquot regeneration; SMAR, simplified multiple aliquot regenerative dose. Our samples were tested at the Key Laboratory of Crustal Dynamics, CEA. Under weak red light, fine quartz grains (4–11 μm) were separated, and the purity was tested by the infrared stimulated luminescence (IRSL) scanning until an IRSL/OSL ratio was less than 3%. The equivalent dose was determined using fine-grained quartz on a RisΦ DA-15-OSL/TL reader. Following the experimental procedures of *Wang et al*. [2010], uranium and thorium contents were determined with a Daybreak 582 thick source alpha counter. The potassium content was measured with a flame photometer.

silt overlying alluvial gravel of terrace T1 at a natural exposure yielded an age of 1.46 ± 0.15 ka (Figure 11c and Table 2), showing that terrace T1 formed earlier than this age. A charcoal sample (LEGW-2011-C-1) collected from the middle part of the overlying gray-black soil on terrace T2 yields an age of 7260 ± 50 cal yr BP (Figure 11c and Table 1), indicating that the T2 terrace formed prior to this age.

4.1.4. Site of Denglongwa Creek (32°31′56.8″N, 102°28′48.3″E)

[52] At Denglongwa creek, the fault zone is composed of two strands 100 m apart marked by two fault scarps on the mountain frontal alluvial fan (Figure 12). The Denglongwa creek appears to be very young because the width of the stream channel is narrow, and no terrace is developed along the valley. A profile across the two fault branches (g-g′ in Figure 12) suggests a vertical displacement of 3.1 ± 0.1 m.

[53] A fault exposure was found where the creek runs through the F1 scarp (Figure 12). The fault dislocated alluvial gravel and is characterized by oriented clasts with a steep dip in the fault shear zone (Figure 13). Away from the fault zone, bedding is relatively planar. The offset alluvial gravel shows a ~1.8 m high scarp. A unit of colluvial deposits at the foot of the scarp is composed of poorly sorted gravel filled with grayish-yellow sand, suggesting that it might be associated with the fault (F1). Unfortunately, we did not find any organic sediment suitable for radiocarbon dating within alluvial or colluvial sediments. Two OSL samples collected from the upper and lower parts of colluvial wedge indicate that the mountain-front alluvial fan formed before ~14 ka (Figure 13 and Table 2). This inference is in agreement with another OSL sample (LRB2-TL2) from the lower part of overlying silt on the alluvial fan near Longri Town that yielded an age of 15.5 ± 1.7 ka [*Xu et al*., 2008].

4.1.5. South of Sizhai Village (32°24′57.9″N, 102°14′56.5″E)

[54] At the southernmost end of the Longriqu fault south of Sizhai Town, Gengqing Gully merges with the Nabuze River (Figure 14). North of the intersection, there is a wide abandoned channel ~6–7 m above the present valley of Gengqing Gully. From the geomorphic characteristics, we infer that Gengqing Gully once flowed along the paleochannel. Because the Longriqu fault offsets the interfluver between the two streams, Gengqing Gully had to abandon its previous channel. The ~500 m dextral offset of the ridge (Figure 14) between the two streams suggests that the Longriba fault has experienced a long history of right-slip motion.

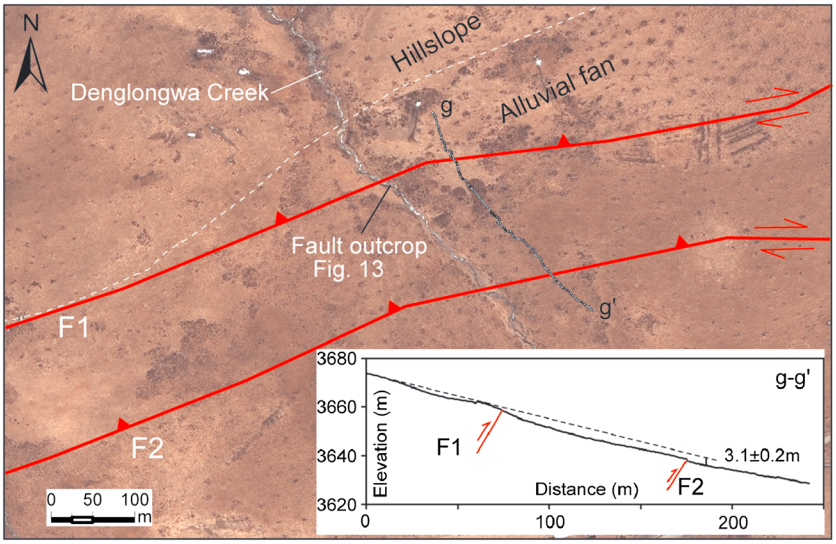

Figure 12. Fault traces and fault scarps on the alluvial fan at the Denglongwa creek. See location in Figure 2. Topographic profile was conducted by RTK GPS.

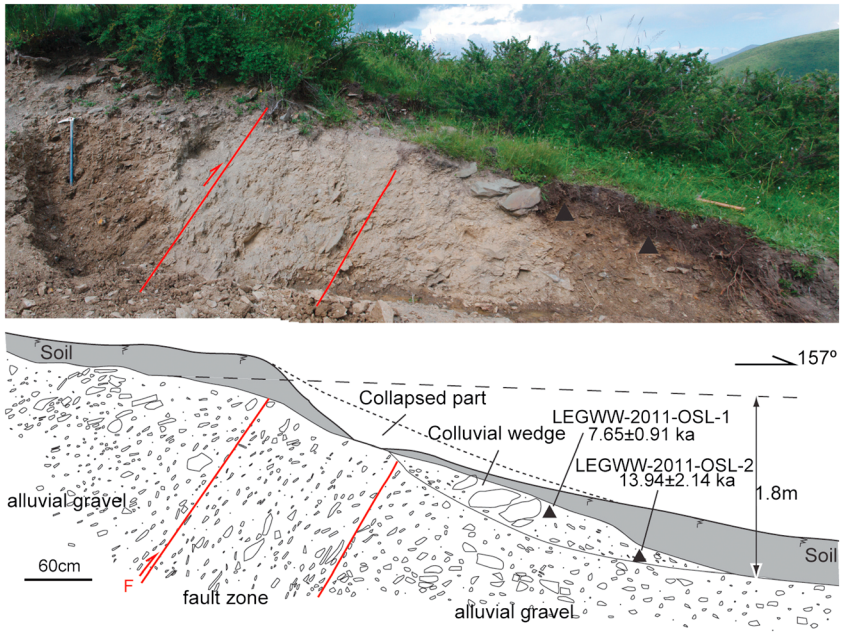

Figure 13. Fault exposure in the alluvial fan at Denglongwa Creek. See location in Figure 12. Fault zone is characterized by oriented clasts.

[55] Northwest of Gengqing Creek, some small creeks generated an alluvial fan along the mountain front (Figure 14), implying that the mountain north of Gengqing Gully might have undergone tectonic uplift. The Longriqu fault cut through the alluvial fan and generated a clear fault scarp. Topographic measurement shows that the fault scarp is 4.0 ± 0.2 m high (Figure 15). A radiocarbon sample collected from the upper part of the alluvial sediments yields an age of 10430 ± 80 cal yr B.P. (Figure 15 and Table 1).

4.1.6. Summary of Slip Rates on the Longriqu Fault

[56] Gailongwa, Longergeng, and Tuokouxia gullies share the same base level and have equivalent terrace heights. So we postulate that their terraces formed approximately at the same time. According to the dating results of river terraces published in this area [*Xu et al.*, 2009], T1 terrace formed in the latest Holocene, T2 formed in the early Holocene, and T3 formed in the latest Pleistocene. From the foregoing discussion and dating results, terraces T2 and T1 formed ~11 ± 0.1 ka and ~2 ka, respectively. The mountain frontal alluvial fan and terrace T3 probably formed concurrently at ~18 ± 0.2 ka. Although these terrace ages provide maximum constraints, they are probably very close to the true terrace ages.

[57] Therefore, the 45 ± 5 m, 46 ± 7 m, and 42 ± 6 m offsets on the T3/T2 riser yield an offset estimate of 44.4 +7.1/−7.0 m with 95% bounds. Along with the ~18 ± 0.2 ka age of terrace T3, a dextral slip rate of 2.5 ± 0.4 mm/yr since ~18 ka is estimated along the Longriqu fault. The 6.8 ± 0.5 m, 2.0 ± 0.2 m, and 3.2 ± 0.2 m vertical displacements on T3 provide a vertical displacement of 0.2 +0.2/−0.1 mm/yr since ~18 ka. The unusual scarp height (~6.8 m) may be associated with the local change of fault strike and complicated fault systems at the Gailongwa site (Figures 2 and 4).

[58] Similarly, the 15 ± 2 m and 16 ± 4 m offsets on the T2/T1 riser yield an offset estimate of 15.3 +4.0/−2.8 m. Along with the ~11 ± 0.1 ka age of T2, a dextral slip rate of 1.4 +0.4/−0.3 mm/yr since ~11 ka is estimated. The 1.5 ± 0.1 m, 0.5 ± 0.1 m, and 0.2 ± 0.1 m vertical displacements on T2 yield a vertical displacement of 0.1 ± 0.1 mm/yr since ~11 ka. These vertical slip rates are apparently smaller than the ~0.4 mm/yr rate south of Sizhai (Figure 15), probably

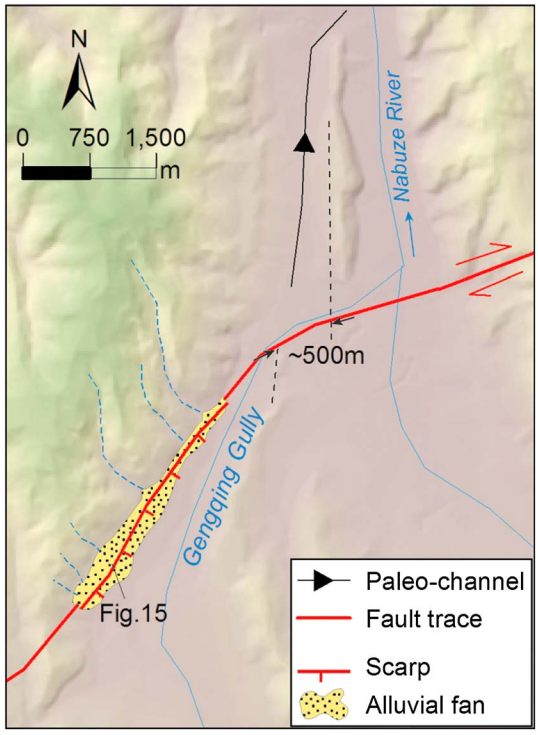

Figure 14. Offset landforms of the southernmost Longriqu fault south of Sizhai Town. See location in Figure 2. The dashed lines show the offset interfluve.

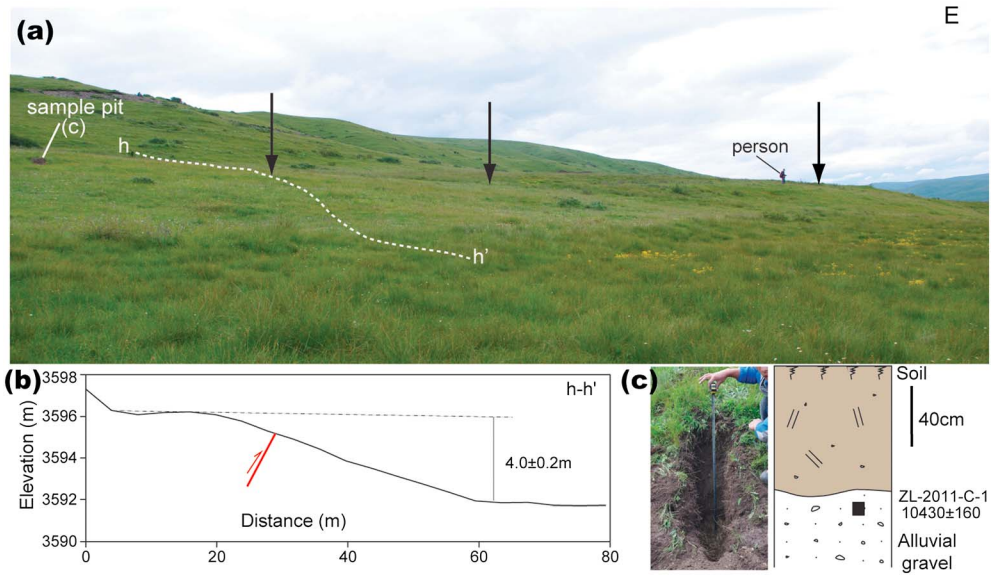

Figure 15. Fault scarp on the alluvial fan of the southernmost Longriba fault. See location in Figure 14. Black arrows indicate fault scarp. Topographical profile across the fault scarp was conducted by RTK GPS. The strata in the sample pit are composed of the gray-black turf in the upper part and alluvial gravel in the lower part.

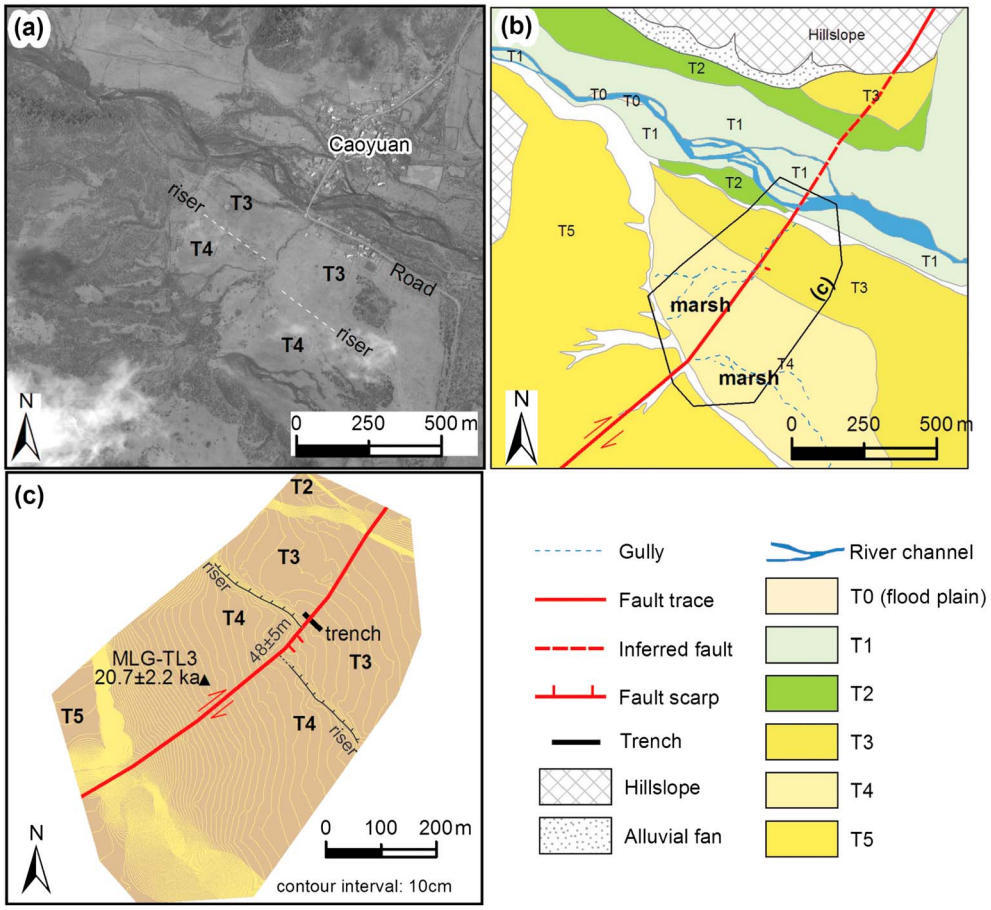

Figure 16. Offset landforms along the Maoergai fault at Caoyuan Village, modified after *Ren et al.* [2013]. See location in Figure 2. (a) WorldView-1 imagery of offset terrace. (b) Geomorphic interpretative map and fault trace. (c) Topographic survey of faulted terrace south of Caoyuan village, conducted by RTK GPS. See location in (b).

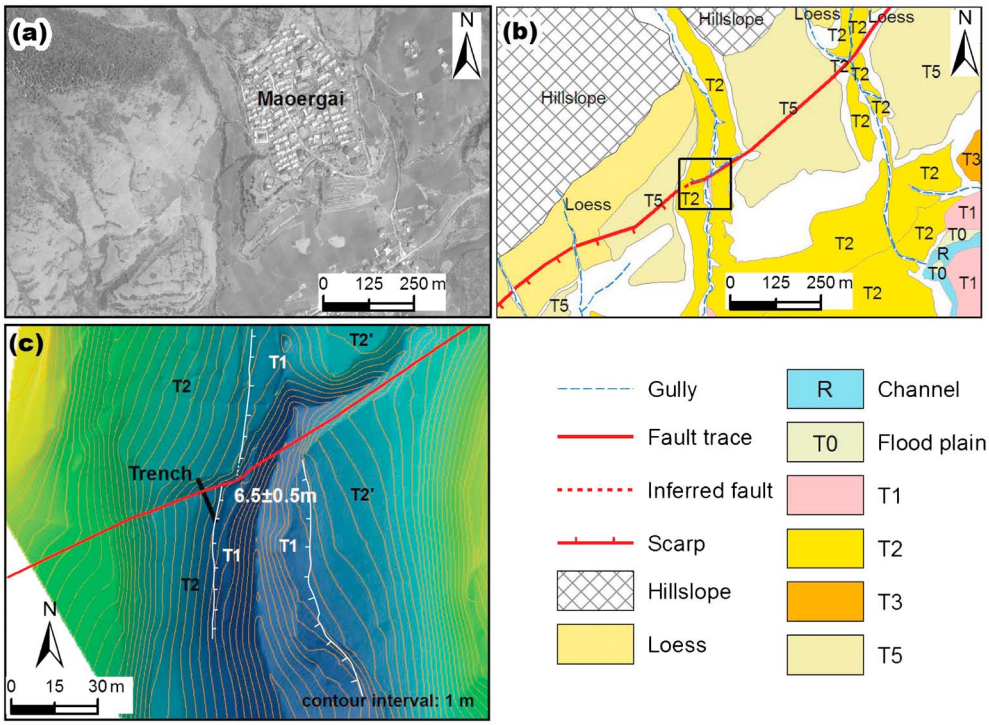

Figure 17. Offset landforms along the Maoergai fault at Maoergai village. See location in Figure 2. (a) WorldView imagery of offset landforms. (b) Geomorphic interpretative map and fault trace, modified after *Ren et al.* [2013]. (c) Topographic survey of faulted terrace southwest of Maoergai village, conducted by RTK GPS. See survey range in Figure 17b. The terrace risers are placed based on the World View imagery and field observations.

associated with the change of fault strike at the southernmost end of the Longriqu fault (Figure 14).

4.2. Maoergai Fault

[59] The Maoergai fault, ~65 ± 5 km long, experiences a pure right-lateral movement. It is characterized by fault valleys and shutter ridges in the southwest and offset streams in the northeast. Detailed work has been done at Caoyuan and Maoergai villages in the northeast of the fault (Figure 2).

[60] At Caoyuan Village, the fault extends through the T3 and T4 terraces of the Maoergai River (Figures 16a and b). The T4/T3 riser was dextrally offset by 48 ± 5 m (Figure 16c). An OSL sample (MEG-TL3) collected from the top of fluvial sands of T4 yields an age of 20.7 ± 2.2 ka (Figure 16c andTable 2). Radiocarbon ages of the sediments in the trench on T3 indicate that T3 formed at 14,350 ± 220 cal yr B.P. [*Ren et al.*, 2013]. Thus, the right-lateral rate of the Maoergai fault since ~21 ka is estimated to 2.3 + 0.4/−0.3 mm/yr, smaller than previous slip rate estimate (3.6 ± 0.5 mm/yr) based on the lower terrace age [*Xu et al.*, 2008]. Topographic mapping shows no obvious vertical offset across the fault (Figure 16c).

[61] At Maoergai Village, the fault offset the gully west of the village (Figure 17). A ~1.4 m high scarp on T2 was attributed to a topographic effect due to the slope (~12°) of the tread of terrace T2 [*Ren et al.*, 2013]. The T2/T1 riser is right-laterally offset by 6.5 ± 0.5 m. A trench on T2 (Figure 17c) shows that T2 probably formed at 9490 ± 90 cal yr B.P. [*Ren et al.*, 2013]. So the dextral slip rate of the Maoergai fault is 0.7 ± 0.1 mm/yr.

5. Discussion

5.1. Rupture Behavior on the Longriba Fault Zone

[62] Our paleoseismic studies indicate that in the latest Quaternary, the Longriqu fault zone has experienced four events (EL1-EL4), which occurred at 5080 ± 90; 11,100 ± 380; 13,000 ± 260; and 17,830 ± 530 cal yr B.P., respectively. Trenching work at Caoyuan and Maoergai villages [*Ren et al.*, 2013] demonstrates a history that three paleoearthquakes (EM1-EM3) since ~14 ka occurred on the Maoergai fault at 5170 ± 80, 7100 ± 70, and 8510 ± 420 cal yr B.P., respectively. Displacement constraints indicate that the paleoseismic histories on both faults are probably complete in the time range discovered by trenching. We plot the events on both faults using the normal probability distribution considering the age mean and 95% bounds (Figure 18). The plot shows that the last event has a good temporal correlation with a small difference of ~90 years.

[63] Two possible mechanisms may be responsible for the two very close surface-rupturing events. First, two events ruptured both fault strands of the Longriba fault zone in a short time, just as the New Madrid fault system where at least three catastrophic earthquakes greater than Mw 7.0 occurred during the winter of 1811 and 1812 [cf. review by *Yeats*, 2012]. They were interpreted to be related to the interaction of adjacent faults by stress triggering [*Kenner et al.*, 2000; *Pratt*, 2012]. The interaction of adjacent faults also includes two cases. In one case, two faults are connected by a small gap at their tips along fault strike, such as a pull-apart basin in a strike-slip fault system. For strike-slip faults, the

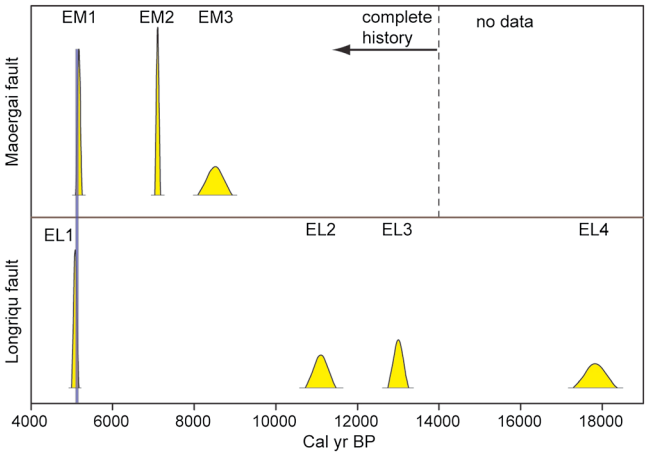

Figure 18. Age correlation of the paleoearthquakes on the Maoergai and Longriqu faults. Paleoseismic data of the Maoergai fault are from *Ren et al*. [2013]. Dashed line shows the upper limit of the complete history along the Maoergai fault. The age of the paleoearthquake is expressed by probability density function of normal distribution with 95% bounds, and the height of the distribution shows the probability of event age [*Weldon et al*., 2005].

width of the gap, an important parameter to determine whether the rupture can propagate across the gap, has been extensively studied along many large-scale strike-slip faults [e.g., *Harris and Day*, 1993; *Lettis et al*., 2002]. The empirical relationships of rupture displacement and gap dimension from coseismic rupture data and numerical analysis [*Duan and Oglesby*, 2006; *Lettis et al*., 2002; *Wesnousky*, 2008] indicated that a fault gap wider than ~5–8 km can impede any fault slip propagation. The distance between the Longriqu and Maoergai faults, however, is ~20–30 km, significantly bigger than the maximum width to arrest the propagation of surface rupture, suggesting that this empirical relation is not applicable to the Longriba fault zone. In another case, a large earthquake on one fault results in stress accommodation on a nearby fault. This case has been observed by stress measurement and has been calculated by numerical modeling in many fault zones. For example, the 2008 Wenchuan earthquake caused an increase of stress on the surrounding faults [*Parsons et al*., 2008; *Wan and Shen*, 2010]. When the stress on a fault is close to critical failure stress, any small increase may trigger the rupture of the fault. But in a parallel fault system, one rupture on a fault will decrease the stress on another fault. Namely, an earthquake will slow down the rupture on another parallel fault. Therefore, stress trigger cannot account for the two very close earthquakes on the Maoergai and Longriqu faults.

[64] Another mechanism is coseismic rupture of two sub-parallel faults during a large earthquake, such as the 2008 Wenchuan earthquake that ruptured both sub-parallel faults, the Yingxiu-Beichuan, and Guanxian-Jiangyou faults with a separation distance of ~10–15 km [*Xu et al*., 2009]. The two faults are regarded as thrust faults with a strike-slip component; they probably merge at depth [*Zhang et al*., 2010]. Numerous studies have suggested that the ongoing eastward motion of the Tibetan Plateau relative to the Sichuan Basin led to the accumulation of the deformation on the merged fault and finally co-ruptured both faults [*Xu et al*., 2009; *Zhang et al*., 2010]. So we infer that the Maoergai and Longriba faults might merge at depth. An enough slip on the merged fault in the seismogenic zone may result in the upward propagation of rupture along the two fault strands.

[65] Another interesting finding is that the Longriqu and Maoergai fault might undergo an alternating activity. Prior to the last event, two events occurred on the Moergai fault during ~6–10 ka, whereas the Longriqu fault was quiescent in this period. During ~10–14 ka, the Maoergai fault was quiescent, while two events ruptured the Longriqu fault. Although no event was discovered prior to 14 ka on the Maoergai fault, a quiescent period for the Longriqu fault during ~14 to ~17 ka (Figure 18) might suggest that the Maoergai fault might be active during this period. This needs to be verified by a further study for a longer paleoseismic history on the Maoergai fault. If we take the Longriqu and Maoergai faults as a whole, the Longriba fault zone appears to undergo a regular recurrence with an interval of ~2000 years before the last event.

[66] The alternation of activity on the two fault branches of the Longriba fault zone may have two implications. First, it suggests that the Longriba and Maoergai faults may merge at depth as the Yingxiu-Beichuan and Guanxian-Jiangyou faults do [*Zhang et al*., 2010]. The eastward motion of the Tibetan Plateau leads to the concentration of strain on the merged fault at depth. Second, the fault zone should be considered as a whole when analyzing the rupture behavior on a fault system. Paleoseismic studies are generally useful to investigate seismic recurrence, especially in the regions where sparse or no surface-rupturing earthquakes occurred in the historic record. For the areas where the fault zone includes several sub-parallel strands, any study trying to discuss the recurrence of large earthquakes on an individual strand of a fault zone may be wrong or may misinterpret fault behavior. For example, if only the Maoergai fault is considered, it will be applicable for a cluster model. It will add the complexity of the models of seismic hazard assessment and might yield a wrong result.

[67] About the reason that these two faults rupture coseismically only in the last earthquake, we infer that the Longriqu fault has accumulated enough strain for a rupture after a long time (>5000 years) following event EL2, while some strain also has been accumulated on the Maoergai fault after >2000 years following event EM2 (Figure 18). When the Longriqu fault ruptured, the seismogenic zone on the merged fault of these two strands at depth was damaged. The strain on the Maoergai fault might reach the critical point of the damaged seismogenic zone and finally caused the rupture of the Maoergai fault together with the Longriqu fault. This case can be seen in the rupture process of the 2008 Wenchuan earthquake. The Yingxiu-Beichuan fault is the main seismogenic fault. The rupture of the 2008 earthquake initiated on the Yingxiu-Beichuan fault, and after several seconds, the Guanxian-Jiangyou fault was also ruptured [*Xu et al*., 2009]. Longer paleoearthquake history is needed to find another possible coseismically rupture event on the Longriqu and Maoergai faults.

[68] In summary, we propose that the last event (E1) might be a larger earthquake which ruptured the Longriqu and Maoergai faults. The quiescent period longer than 5000 years after the last event is interpreted to balance with its larger magnitude.

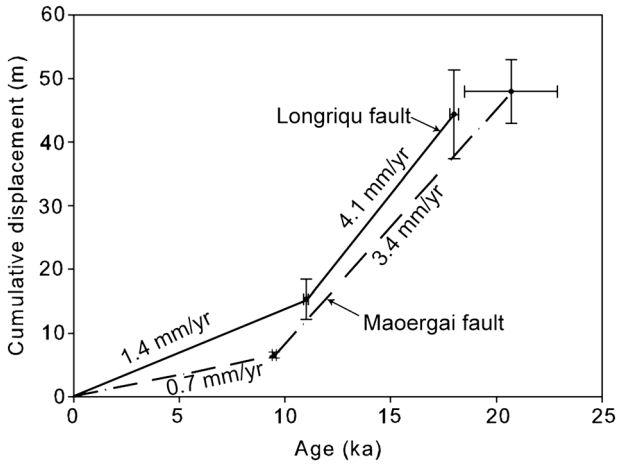

Figure 19. Temporal variation of right-lateral slip rates along the Longriqu and Maoergai faults. Terrace ages are according to radiocarbon and OSL dating. Fault offsets are based on topographic survey of displaced terrace riser.

5.2. Slip Rates Along the Longriba Fault Zone

[69] Our result indicates that the dextral rate along the Longriqu fault since ~18 ka is 2.5 ± 0.4 mm/yr but is 1.4 +0.4/−0.3 mm/yr since ~11 ka. Its vertical slip rate is very small (0.1–0.2 mm/yr), demonstrating that the Longriqu fault is predominantly strike slip. On the Maoergai fault, the dextral rate since ~21 ka is 2.3 +0.4/−0.3 mm/yr but is 0.7 ± 0.1 mm/yr since ~9.5 ka. These results indicate that the whole Longriba fault zone is dominantly right-lateral motion accompanying a very small south-verging thrust component on the Longriqu fault, consistent with the result of *Xu et al*. [2008].

[70] However, our slip rates on both faults are smaller than that of *Xu et al*. [2008], because they assigned the age of the lower terrace to the offset riser. For example, at Caoyuan Village, a 48 ± 5 m offset of T4/T3 riser yields a ~3.4 mm/yr dextral slip rate for the Maoergai fault if using the age of the lower terrace. The trench on terrace T3 [*Ren et al.*, 2013] indicates only three surface-rupturing events since the formation of terrace T3. If the lower terrace is responsible for the terrace riser, it will yield a mean coseismic slip of ~16 m, equivalent to Mw ~8 based on the empirical relation of coseismic slip and magnitude on strke-slip faults [*Wells and Coppersmith*, 1994]. This is evidently incompatible with the length of the Maoergai fault ($\sim 65 \pm 5$ km).

[71] Also, our results show that the slip rate on the Longriba fault zone is not temporally uniform. We use the sum of slip rates on the Maoergai and Longriqu faults to discuss the variation of slip rates on the Longriba fault zone. The dextral rate since the latest Quaternary is ~4.8 mm/yr, whereas the dextral rate in the Holocene is ~2.1 mm/yr. If we subtract the Holocene offset from the latest Quaternary offset, the slip rate in the latest Pleistocene is up to ~7.5 mm/yr, indicating an apparent decrease of slip rate on the Longriba fault zone from latest Pleistocene to the Holocene (Figure 19). There are three possible reasons accounting for the decrease of slip rate.

[72] The first possible reason is that the Longriba fault zone is getting less active in the Holocene. But it does not coincide with the results derived from GPS measurement and numerical models. The GPS velocity field shows a clear shear zone along the Longriba fault zone, although the GPS station near the fault is sparse (Figure 20). Numerous GPS models have been built to analyze slip rates on major faults around the Tibetan Plateau [*Gan et al*., 2007; *Thatcher*, 2007; *Zhang et al*., 2004]. In these models, the Bayan Har block was generally regarded as one block because the active Longriba fault zone had not been identified at that time. Recently, *Cheng et al*. [2012] divided eastern Tibet into 11 sub-blocks based on characteristics of active faults,

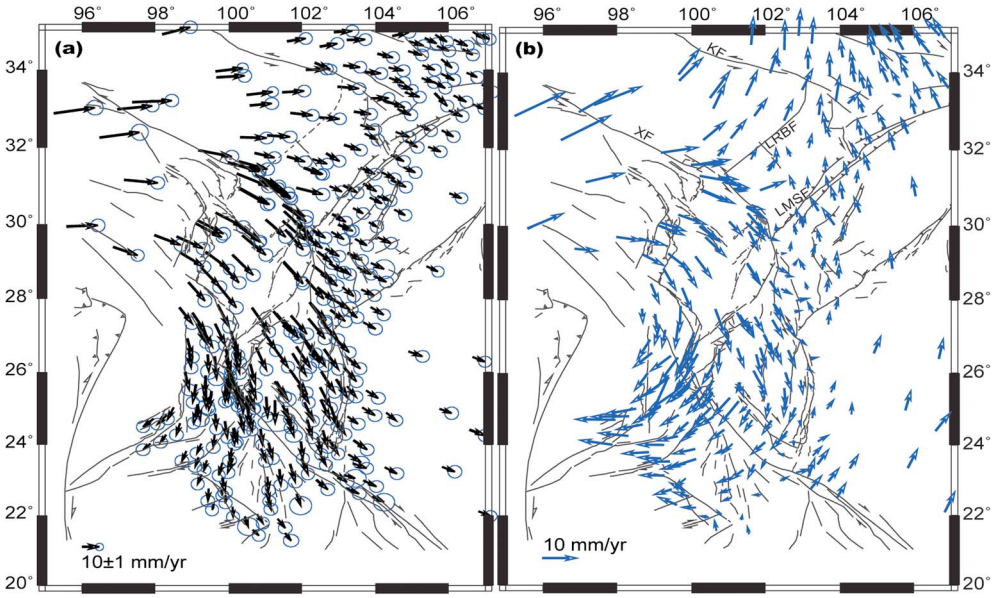

Figure 20. GPS velocity in eastern Tibet and adjacent regions. (a) Present-day crustal movement relative to Eurasia. GPS data are from *Gan et al*. [2007]. The ellipse at the tip of each velocity vector is 95% confidence. (b) Present-day crustal interior deformation field of eastern Tibet after the rigid rotation of the whole Plateau was taken out. Euler pole: 29.3°N, 34.5°E. Rotation angle: −0.11°/Ma. Data are from *Cheng et al*. [2012].

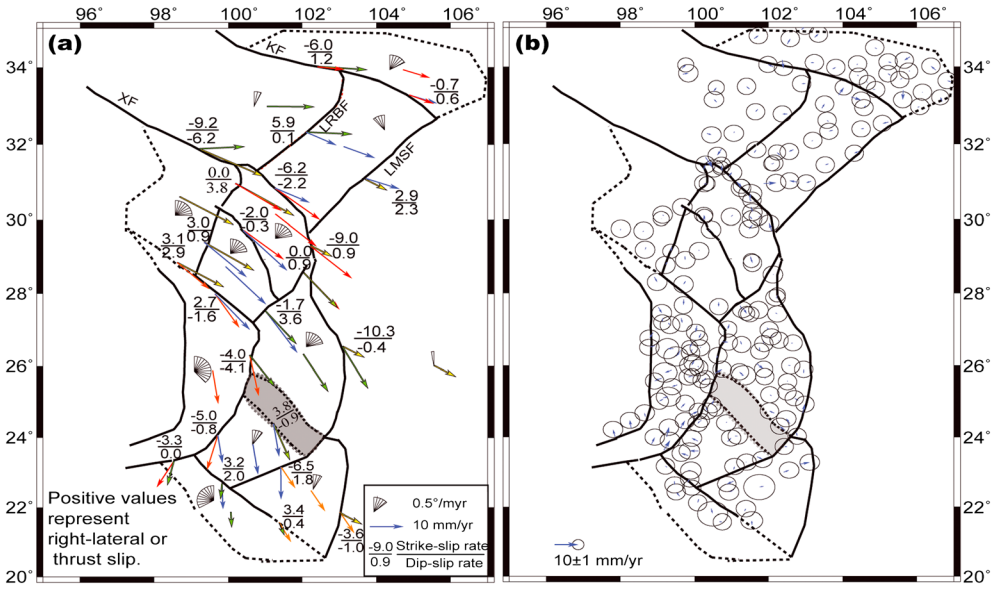

Figure 21. Sub-block motion (a) vectors and (b) residuals of the eastern margin of the Tibetan Plateau, based on rigid sub-block model. Data are from *Cheng et al*. [2012]. Sub-block motion vectors are expressed by different colors and are also put on the boundaries of the sub-blocks to compare with adjacent sub-blocks. See abbreviations for active faults in Figure 1b.

historical earthquakes, and focal mechanism data as shown in Figure 1b. The Bayan Har block is separated into the Aba and Longmen Shan sub-blocks by the Longriba fault zone. The rigid motion of all the sub-blocks and slip rates of their boundary faults based on their sub-block model suggested a dominantly dextral slip of 5.9 mm/yr and only a small thrust slip of 0.1 mm/yr on the Longriba fault zone (Figure 21), approximately consistent with our geological result. GPS rates represent the present-day deformation across the fault, suggesting that the Longriba fault zone is not becoming inactive but remains very active. Several decades of measurement suggest a relatively steady motion in eastern Tibet, although little is known about the long-term variation of GPS rate [*Gan et al*., 2007; *Shen et al*., 2005; *Zhang et al*., 2004].

[73] The second is that it may be related to the seismic cycle. From our paleoseismic results, the last event ruptured the Longriba fault zone ~5000 years ago. Such a long time may dilute the accumulated offset in early Holocene. If we subtract this long elapsed time in the calculation of the slip rate, the Longriba fault zone will have a ~4.0 mm/yr rate during the Holocene. This value is roughly comparable to the GPS result (Figure 21). It also suggests that a long elapsed time should be considered when comparing long-term geologic slip rates with short-term GPS rates. However, the difference in slip rate from late Pleistocene to the Holocene is still there.

[74] The third is probably associated with the slowing-down eastern motion of the Tibetan Plateau. This decrease of slip rate can also be found along the Longmen Shan fault zone. At Yingxiu town, the fault dislocated terraces T4–T1 of Minjiang River. The heights of fault scarps on these terraces are ~40, ~16, ~10, and ~3 m, respectively [*Dong et al*., 2008]. Amongst them, the youngest terrace (T1) merely documented the coseismic displacement for the 2008 earthquake. The ages of T4 and T2 dated by TL (thermoluminescence) and radiocarbon formed at ~75 and ~20 ka, respectively [*Li et al*., 2006; *Ma et al*., 2005]. The displacement of the 2008 earthquake is subtracted from the multiple offset to estimate slip rates. During 75 to 20 ka, the fault vertical slip rate is ~0.55 mm/yr, whereas since 20 ka, the rate decreases to ~0.35 mm/yr. The drop of slip rate on the Longmen Shan fault zone appears to somewhat lag behind that on the Longriba fault zone, possibly related to the delayed effect of deformation propagation. Thus, we propose that the slowing down of eastern motion of the Tibetan Plateau may be responsible for the decrease of slip rates on the Longriba fault zone. But further studies are needed on the mechanism of the decreased eastern motion of the Tibetan Plateau.

[75] In addition, the difference between the Holocene geological and GPS rates implies that the Longriba fault zone might have been locked since the last event. The GPS rate may represent the interseismic accumulation rate of strain along the fault. If only one of the individual faults is ruptured, the moment magnitude (Mw) for both fault strands is estimated to ~7.2–7.4 [*Wells and Coppersmith*, 1994]. If a rupture of both faults is considered, the Longriba fault zone will experience a large earthquake of Mw ~7.6 [*Wells and Coppersmith*, 1994]. The moment accumulated on the Longriba fault zone is enough for the next large earthquake after over 5000 years. So we propose that there is a high possibility that a large earthquake bigger than Mw 7 will rupture the Longriba fault zone in the near future.

5.3. The Role of the Longriba Fault Zone in Strain Partitioning in Eastern Tibet

[76] From the aspect of long-term geological slip rate, the Longriba fault zone has a >4 mm/yr dextral rate (Figure 19), while the Longmen Shan fault zone accommodates less than ~3 mm/yr thrust and ~2 mm/yr dextral slip rate [*Densmore et al*., 2007; *Li et al*., 2006; *Ma et al*., 2005]. The short-term

GPS result also suggests that the Longriba fault zone has a slip rate similar to the Longmen Shan fault zone (Figure 21), suggesting an important role in strain partitioning taken by the Longriba fault zone.

[77] GPS measurements indicates that the Tibetan Plateau is moving due eastward and is resisted by the Longriba and Longmen Shan fault zones in eastern Tibet [*Gan et al*., 2007]. However, the Longriba and Longmen Shan fault zones strike N ~ 60ºE. Thus, the oblique motion of the interior Plateau with the two fault zones will be resolved into two portions. One portion is transformed into dextral slip along the Longriba fault zone. Another portion continues to move southeastward and collides with the rigid Sichuan Basin to cause uplift and produce thrusting and dextral slip on the Longmen Shan fault zone. The relatively soft Longmen Shan sub-block accommodates the compression between the Tibetan Plateau and Sichuan Basin and results in folding and uplift of mountains between the Longriba and Longmen Shan fault zones. The steep dip on the Longriba fault zone enables the strike-slip motion, whereas the relatively gentle dip on the Longmen Shan fault zone results in the thrust motion.

[78] A recently accomplished deep seismic reflection profile was conducted across the Longriba and Longmen Shan fault zones [*Gao et al*., 2012], in which the Longriqu and Maoergai faults merge as a fault in the upper crust, consistent with our proposal from paleoseismologic results (sections 5.1 and 5.2). The Longriba fault zone, along with the Longmen Shan fault zone, was proposed to link with a detachment fault characterized by a low-velocity layer at ~20 km depth [*Hubbard and Shaw*, 2009; *Wang et al*., 2007]. This seismic reflection profile also showed that the Moho beneath the Longriba fault zone is displaced, suggesting that it has a long history and can be as a boundary of the sub-blocks. In this profile, the Moho beneath the Longmen Shan appears to dive under the Moho beneath the Sichuan Basin, probably resulting in the uplift of the basin that may account for the erosion of the Sichuan basin in Cenozoic time and the lack of a typical foredeep basin related to the steep topography along the Longmen Shan [*Royden et al*., 2008]. Detailed results await the detailed explanation of this deep seismic profile [*Gao et al*., 2012].

[79] Although there is a vigorous debate on two models for the uplift of eastern Tibet, the lower crustal flow model proposes that the deformation of thrust faults in the upper crust is decoupled from the mantle lithosphere, apparently inconsistent with the deep seismic reflection profile [*Gao et al*., 2012]. Although the result of some studies [*Wang et al*., 2012] was thought to favor the lower crustal flow, increasing evidence has been recently reported to support the brittle crustal thickening model. For example, *Hubbard and Shaw* [2009] used balanced cross sections to infer that crustal shortening alone is sufficient to illustrate the crustal thickness of the Longmen Shan. *Lease et al*. [2012] exploited balanced cross sections combined with thermochronological and magnetostratigraphic constraints to propose that lower crustal flow is not necessary in northeastern Tibet.

[80] Finally, I propose a model to illustrate the kinematic mechanism in eastern Tibet (Figure 22). The Longmen Shan sub-block is under the combined action of eastward extrusion from the Tibetan Plateau and northwestward push of the Sichuan Basin, resulting in dextral slip along the Longriba fault zone and thrust slip with dextral component along the Longmen Shan. Although the Longmen Shan fault zone undoubtedly plays an important role in absorbing deformation in eastern Tibet, the strike-slip Longriba fault zone probably also takes an equally important role in strain partition. This geometry is somewhat similar to that proposed for subduction zones, such as New Guinea [*Abers and McCaffrey*, 1988], Sumatra, Japan, and San Andreas [cf. summary of *Yeats*, 2012], where the subduction is oblique, the strike-slip component commonly is absorbed not by oblique thrusting but by pure strike-slip faulting on a fault that occurs on the rear of the thrust belt. But this model still needs further geophysical evidence and geodynamic modeling.

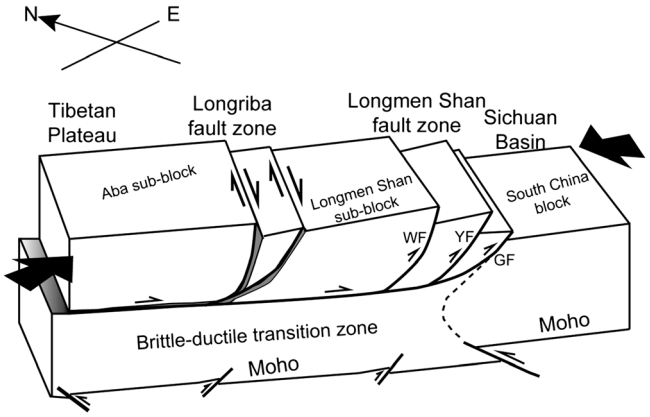

Figure 22. Schematic block diagram showing the proposed kinematic mechanism along the Longriba and Longmen Shan fault zones. The relationships of active faults and the Moho are according to the deep seismic results [*Gao et al*., 2012; *Hubbard and Shaw*, 2009; *Wang et al*., 2007]. Black arrows indicate directions of force acted on the Longmen Shan sub-block derived from GPS results [*Gan et al*., 2007; *Zhang et al*, 2004]. GF, Guanxian-Jiangyou fault; WF, Wenchuan-Maoxian fault; YF, Yingxiu-Beichuan fault.

6. Conclusions

[81] Based on field investigations, topographic surveys, and numerical dating, we draw the following conclusions:

[82] 1. The Longriba fault zone undergoes oblique motion with dominantly dextral and a small southeast-verging reverse component.

[83] 2. Four surface-rupturing events occurred on the Longriqu fault at 5080 ± 90; $11{,}100 \pm 380$; $13{,}000 \pm 260$; and $17{,}830 \pm 530$ cal yr B.P. The last event probably ruptured the Longriqu and Maoergai faults. Prior to the last event, the two strands of the Longriba fault zone appear to experience an alternating activity. The Longriba fault zone has a high potential for a large earthquake.

[84] 3. The slip rate of the Longriba fault zone decreases from ~7.5 mm/yr in latest Pleistocene to ~2.1 mm/yr in the Holocene. The drop is probably related to the slowdown of the eastern motion of the Tibetan Plateau.

[85] 4. The two branches of the Longriba fault zone may merge in the mid-upper crust with a steep dip. This fault zone, along with the Longmen Shan fault zone, is responsible

for the deformation of the Longmen Shan sub-block. The Longriba fault zone also plays an important part in strain partitioning in eastern Tibet.

[86] **Acknowledgments.** This research was funded jointly by the National Science Foundation of China (grant 41102134), Institute of Crustal Dynamics, China Earthquake Administration Research Fund (grant ZDJ2013-23, ZDJ2009-01), and the Scientific Investigation Project of Yushu Earthquake. We thank W. Kang, R. Ding, Z. Gong and S. Liu for field assistance; J. Zhao for OSL analyses; and A. Meigs, J. Nabelek, and E. Guerrero for discussions. We also thank J. Cheng for sharing his modeled GPS data and Christopher Ramsey for discussing the use of software OxCal. Thoughtful reviews by C. DuRoss, A. Carter, and one anonymous reviewer improved the manuscript.

References

Abers, G., and R. McCaffrey (1988), Active deformation in the New Guinea fold-and-thrust belt: Seismological evidence for strike-slip faulting and basement-involved thrusting, *J. Geophys. Res.*, *93*(B11), 13332–13354, doi:10.1029/JB093iB11p13332.

Bird, P. (1991), Lateral extrusion of lower crust from under high topography in the isostatic limit, *J. Geophys. Res.*, *96*(B6), 10275–10286, doi:10.1029/91jb00370.

Bronk Ramsey, C. (2008), Deposition models for chronological records, *Quat. Sci. Rev.*, *27*(1), 42–60, doi:10.1016/j.quascirev.2007.01.019.

Burchfiel, B., Z. Chen, Y. Liu, and L. Royden (1995), Tectonics of the Longmen Shan and adjacent regions, Central China, *Int. Geol. Rev.*, *37*, 661–735, doi:10.1080/00206819509465424.

Chen, S., and C. J. L. Wilson (1996), Emplacement of the Longmen Shan Thrust—Nappe Belt along the eastern margin of the Tibetan Plateau, *J. Struct. Geol.*, *18*(4), 413–430, doi:10.1016/0191-8141(95)00096-V.

Cheng, J., X. Xu, W. Gan, W. Ma, W. Chen, and Y. Zhang (2012), Block model and dynamic implication from the earthquake activities and crustal motion in the southeastern margin of Tibetan Plateau, *Chinese J. Geophys.*, *55*(4), 1198–1212, doi:10.6038/j.issn.0001-5733.2012.04.016.

China Earthquake Administration (1999a), Historical Strong Earthquake Catalog of China (2300 BC–1911 AD) (in Chinese), Earthquake Publishing House, Beijing.

China Earthquake Administration (1999b), Recent Earthquake Catalog of China (1912–1990, Ms≥4.7) (in Chinese), Chinese Sciences and Technology Press, Beijing.

Clark, M. K., and L. H. Royden (2000), Topographic ooze: Building the eastern margin of Tibet by lower crustal flow, *Geology 28*(8), 703–706, doi:10.1130/0091-7613(2000)28<703:tobtem>2.0.co;2.

Cowgill, E. (2007), Impact of riser reconstructions on estimation of secular variation in rates of strike-slip faulting: Revisiting the Cherchen River site along the Altyn Tagh Fault, NW China, *Earth Planet. Sci. Lett.*, *254*(3–4), 239–255, doi:10.1016/j.epsl.2006.09.015.

Densmore, A. L., M. A. Ellis, Y. Li, R. Zhou, G. S. Hancock, and N. Richardson (2007), Active tectonics of the Beichuan and Pengguan faults at the eastern margin of the Tibetan Plateau, *Tectonics 26*(4), 1–17, doi:10.1029/2006TC001987.

Dong, S., Z. Han, and Y. An (2008), Surface deformation at the epicenter of the May 12, 2008 Wenchuan M8 Earthquake, at Yingxiu Town of Sichuan Province, China, *Sci. China, Ser. E*, *51*(0), 154–163, doi:10.1007/s11431-008-6007-0.

Duan, B., and D. D. Oglesby (2006), Heterogeneous fault stresses from previous earthquakes and the effect on dynamics of parallel strike-slip faults, *J. Geophys. Res.*, *111*(B05309), doi:10.1029/2005JB004138.

DuRoss, C. B., S. F. Personius, A. J. Crone, S. S. Olig, and W. R. Lund (2011), Integration of paleoseismic data from multiple sites to develop an objective earthquake chronology: Application to the Weber segment of the Wasatch fault zone, Utah, *Bull. Seismol. Soc. Am.*, *101*(6), 2765–2781, doi:10.1785/120110102.

Fletcher, K. E. K., T. K. Rockwell, and W. D. Sharp (2011), Late Quaternary slip rate of the southern Elsinore fault, Southern California: Dating offset alluvial fans via 230Th/U on pedogenic carbonate, *J. Geophys. Res.*, *116*(F2), doi:10.1029/2010jf001701.

Gan, W., P. Zhang, Z. K. Shen, Z. Niu, M. Wang, Y. Wan, D. Zhou, and J. Cheng (2007), Present-day crustal motion within the Tibetan Plateau inferred from GPS measurements, *J. Geophys. Res.*, *112*(B8), doi:10.1029/2005JB004120.

Gao, X., R. Gao, G. R. Keller, and X. Xu (2012), Tectonic interactions between the Yangtze block and Songpan-Ganze terrane: New constraints from deep seismic reflection and refraction profiles, as well as magnetic and gravity evidence (with abstract), in 2012 SSA Annual Meeting, edited, p. 429, Seismological Research Letters, San Diego.

Geological Bureau of Sichuan Province (1991), Regional Geology of Sichuan Province (in Chinese), Geological Press, Beijing.

Gold, R. D., E. Cowgill, J. R. Arrowsmith, X. Chen, W. D. Sharp, K. M. Cooper, and X.-F. Wang (2011), Faulted terrace risers place new constraints on the late Quaternary slip rate for the central Altyn Tagh fault, northwest Tibet, *Geol. Soc. Am. Bull.*, *123*(5–6), 958–978, doi:10.1130/b30207.1.

Harris, R. A., and S. M. Day (1993), Dynamics of fault interaction: Parallel strike-slip faults, *J. Geophys. Res.*, *98*(B3), 4461–4472, doi:10.1029/92jb02272.

Huang, W. Q., W. X. Li, and X. F. Cao (1994), Research on completeness of earthquake data in the Chinese mainland (II)—The regional distribution of the beginning years of basically complete earthquake data, *Acta. Seismol. Sin.*, *7*(4), 529–538, doi:10.1007/BF02650738.

Hubbard, J., and J. H. Shaw (2009), Uplift of the Longmen Shan and Tibetan plateau, and the 2008 Wenchuan (M=7.9) earthquake, *Nature 458*(7235), 194–197, doi:10.1038/nature07837.

Jia, S., X. Zhang, J. Zhao, F. Wang, C. Zhang, Z. Xu, J. Pan, Z. Liu, S. Pan, and G. Sun (2010), Deep seismic sounding data reveal the crustal structures beneath Zoigê basin and its surrounding folded orogenic belts, *Sci. China Earth. Sci.*, *53*(2), 203–212, doi:10.1007/s11430-009-0166-0.

Kenner, S. J., Segall, and Paul (2000), A mechanical model for intraplate earthquakes: Application to the New Madrid seismic zone, *Science 289*(5488), 2329–2332, doi:10.1126/science.289.5488.2329.

Kirby, E., N. Harkins, E. Wang, X. Shi, C. Fan, and D. Burbank (2007), Slip rate gradients along the eastern Kunlun fault, *Tectonics 26*(TC2010), doi:10.1029/2006tc002033.

Lease, R. O., D. W. Burbank, H. Zhang, J. Liu, and D. Yuan (2012), Cenozoic shortening budget for the northeastern edge of the Tibetan Plateau: Is lower crustal flow necessary?, *Tectonics 31*(TC3011), doi:10.1029/2011tc003066.

Lensen, G. J. (1968), Analysis of progressive fault displacement during downcutting at the Branch River terraces, South Island, New Zealand, *Geol. Soc. Am. Bull.*, *79*(5), 545–556, doi:10.1130/0016-7606(1968)79[545:aopfdd]2.0.co;2.

Lettis, W., J. Bachhuber, R. Witter, C. Brankman, C. E. Randolph, A. Barka, W. D. Page, and A. Kaya (2002), Influence of releasing step-overs on surface fault rupture and fault segmentation: Examples from the 17 August 1999 İzmit Earthquake on the north Anatolian fault, Turkey, *Bull. Seismol. Soc. Am.*, *92*(1), 19–42, doi:10.1785/0120000808.

Li, Y., R. Zhou, A. L. Densmore, and M. A. Ellis (2006), Geomorphic evidence for the Late Cenozoic strike-slipping and thrusting in Longmen Mountain at the eastern margin of the Tibetan Plateau, *Quat. Res. (in Chinese)*, *26*(1), 40–51.

Lienkaemper, J. J., and C. Bronk Ramsey (2009), OxCal: Versatile tool for developing paleoearthquake chronologies—A primer, *Seismol. Res. Lett.*, *80*(3), 431–434, doi:10.1785/gssrl.1780.1783.1431.

Ma, B., G. Su, Z. Hou, and S. Shu (2005), Late Quaternary slip rate in the central part of the Longmenshan Fault Zone from terrace deformation along the Minjiang River (in Chinese with English abstract), *Seismol. Geol.*, *27*(2), 234–242.

Mason, D. P. M., T. A. Little, and R. J. Van Dissen (2006), Rates of active faulting during late Quaternary fluvial terrace formation at Saxton River, Awatere fault, New Zealand, *Geol. Soc. Am. Bull.*, *118*(11-12), 1431–1446, doi:10.1130/b25961.1.

McCalpin, J. (2009), Paleoseismology, Academic Press.

Mériaux, A. S., et al. (2005), The Aksay segment of the northern Altyn Tagh fault: Tectonic geomorphology, landscape evolution, and Holocene slip rate, *J. Geophys. Res.*, *110*(B04404), doi:10.1029/2004jb003210.

Molnar, P., and P. Tapponnier (1975), Cenozoic tectonics of Asia: Effects of a continental collision, *Science 189*(4201), 419–426, doi:10.1126/science.1189.4201.1419.

Ortuño, M., E. Masana, E. García-Meléndez, J. Martínez-Díaz, P. Štěpančíková, P. P. Cunha, R. Sohbati, C. Canora, J.-P. Buylaert, and A. S. Murray (2012), An exceptionally long paleoseismic record of a slow-moving fault: The Alhama de Murcia fault (Eastern Betic shear zone, Spain), *Geol. Soc. Am. Bull.*, *124*(9-10), 1474–1494, doi:10.1130/b30558.1.

Parsons, T., C. Ji, and E. Kirby (2008), Stress changes from the 2008 Wenchuan earthquake and increased hazard in the Sichuan basin, *Nature 454*(7203), 509–510, doi:10.1038/nature07177.

Peltzer, G., and F. Saucier (1996), Present-day kinematics of Asia derived from geologic fault rates, *J. Geophys. Res.*, *101*(B12), 27943-27956, doi:10.1029/96JB02698.

Pratt, T. L. (2012), Kinematics of the New Madrid seismic zone, central United States, based on stepover models, *Geology 40*(4), 371–374, doi:10.1130/g32624.1.

Reimer, P., M. Baillie, E. Bard, A. Bayliss, J. Beck, P. Blackwell, C. Bronk Ramsey, C. Buck, G. Burr, and R. Edwards (2009), IntCal09 and Marine09 radiocarbon age calibration curves, 0–50,000 years cal BP, *Radiocarbon 51*(4), 1111–1150.

Ren, J., G. Chen, X. Xu, S. Zhang, and C. Mao (2010), Surface rupture of the 2008 Wenchuan, China, earthquake in the Qingping stepover determined from geomorphologic surveying and excavation, and its tectonic implications, *Bull. Seismol. Soc. Am.*, *100*(5B), 2651–2659, doi:10.1785/0120090267.

Ren, J., X. Xu, X. Sun, X. Tan, K. Li, W. Kang, and B. Liu (2012), Geological and geophysical evidences of late Quaternary activity of the range-front fault along the mid-segment of the Longmen Shan thrust belt, *Chinese J. Geophys.*, *55*(6), 1929–1941, doi:10.6038/j.issn.0001-5733.2012.06.014.

Ren, J., X. Xu, R. S. Yeats, S. Zhang, R. Ding, and Z. Gong (2013), Holocene paleoearthquakes of the Maoergai fault, eastern Tibet, *Tectonophysics*, doi:10.1016/j.tecto.2013.01.017, in press.

Royden, L. H., B. C. Burchfiel, and R. D. van der Hilst (2008), The geological evolution of the Tibetan Plateau, *Science 321*(5892), 1054–1058, doi:10.1126/science.1155371.

Shen, Z. K., J. Lu, M. Wang, and R. Burgmann (2005), Contemporary crustal deformation around the southeast borderland of the Tibetan Plateau, *J. Geophys. Res.*, *110*(B11409), doi:10.1029/2004JB003421.

Tapponnier, P., and P. Molnar (1977), Active faulting and tectonics in China, *J. Geophys. Res.*, *82*(20), 2905–2930, doi:10.1029/JB082i020p02905.

Tapponnier, P., Z. Xu, F. Roger, B. Meyer, N. Arnaud, G. Wittlinger, and J. Yang (2001), Oblique stepwise rise and growth of the Tibet Plateau, *Science 294*(5547), 1671–1677, doi:10.1126/science.105978.

Thatcher, W. (2007), Microplate model for the present-day deformation of Tibet, *J. Geophys. Res.*, *112*(B01401), doi:10.1029/2005JB004244.

Wan, Y., and Z.-K. Shen (2010), Static Coulomb stress changes on faults caused by the 2008 Mw 7.9 Wenchuan, China earthquake, *Tectonophysics*, *491*(1–4), 105–118, doi:10.1016/j.tecto.2010.03.017.

Wang, C., W. Han, J. Wu, H. Lou, and W. W. Chan (2007), Crustal structure beneath the eastern margin of the Tibetan Plateau and its tectonic implications, *Journal of Geophysical Research: Solid Earth*, *112*(B07307), doi:10.1029/2005jb003873.

Wang, E., E. Kirby, K. P. Furlong, M. van Soest, G. Xu, X. Shi, P. J. J. Kamp, and K. V. Hodges (2012), Two-phase growth of high topography in eastern Tibet during the Cenozoic, *Nature Geosci*, *5*(9), 640–645, doi:10.1038/ngeo1538.

Wang, M., D. Jia, A. Lin, L. Shen, G. Rao, and Y. Li (2013), Late Holocene activity and historical earthquakes of the Qiongxi thrust fault system in the southern Longmen Shan fold-and-thrust belt, eastern Tibetan Plateau, *Tectonophysics*, *584*, 102–113, doi:10.1016/j.tecto.2012.08.019.

Wang, P., H. Jiang, D. Yuan, X. Liu, and B. Zhang (2010), Optically stimulated luminescence dating of sediments from the Yellow River terraces in Lanzhou: Tectonic and climatic implications, *Quaternary Geochronology*, *5*(2–3), 181–186, doi:10.1016/j.quageo.2009.05.009.

Weldon, R. J., T. E. Fumal, G. P. Biasi, and K. M. Scharer (2005), Past and future earthquakes on the San Andreas fault, *Science 308*(5724), 966–967, doi:10.1126/science.1111707.

Wells, D. L., and K. J. Coppersmith (1994), New empirical relationships among magnitude, rupture length, rupture width, rupture area, and surface displacement, *Bull. Seismol. Soc. Am.*, *84*(4), 974–1002.

Wesnousky, S. G. (2008), Displacement and geometrical characteristics of earthquake surface ruptures: Issues and implications for seismic-hazard analysis and the process of earthquake rupture, *Bull. Seismol. Soc. Am.* , *98*(4), 1609–1632, doi:10.1785/0120070111.

Xu, X., X. Wen, G. Chen, and G. Yu (2008), Discovery of the Longriba fault zone in eastern Bayan Har Block, China and its tectonic implication, *Sci. China. Ser. D-Earth Sci.*, *51*(9), 1209–1223, doi:10.1007/s11430-008-0097-1.

Xu, X., X. Wen, G. Yu, G. Chen, Y. Klinger, J. Hubbard, and J. Shaw (2009), Coseismic reverse-and oblique-slip surface faulting generated by the 2008 Mw 7.9 Wenchuan earthquake, China, *Geology 37*(6), 515–518, doi:10.1130/G25462A.1.

Yeats, R. (2012), Active Faults of the World, Cambridge University Press, Cambridge.

Yeats, R., K. E. Sieh, and C. R. Allen (1997), The Geology of Earthquakes, Oxford University Press, New York.

Yin, A. (2010), Cenozoic tectonic evolution of Asia: A preliminary synthesis, *Tectonophysics*, *488*(1–4), 293–325, doi:10.1016/j.tecto.2009.06.002.

Zechar, J. D., and K. L. Frankel (2009), Incorporating and reporting uncertainties in fault slip rates, *J. Geophys. Res.*, *114*(B12407), doi:10.1029/2009JB006325.

Zhang, P. (2013), A review on active tectonics and deep crustal processes of the Western Sichuan region, eastern margin of the Tibetan Plateau, *Tectonophysics*, *584*, 7–22, doi:10.1016/j.tecto.2012.02.021.

Zhang, P., P. Molnar, and X. Xu (2007), Late Quaternary and present-day rates of slip along the Altyn Tagh Fault, northern margin of the Tibetan Plateau, *Tectonics 26*(5), doi:10.1029/2006tc002014.

Zhang, P., X. Wen, Z. K. Shen, and J. Chen (2010), Oblique, high-angle, listric-reverse faulting and associated development of strain: The Wenchuan earthquake of May 12, 2008, Sichuan, China, *Annu. Rev. Earth Planet. Sci.*, *38*, 353–382, doi:10.1146/annurev-earth-040809-152602.

Zhang, P., Z. Shen, M. Wang, W. Gan, R. Bürgmann, P. Molnar, Q. Wang, Z. Niu, J. Sun, and J. Wu (2004), Continuous deformation of the Tibetan Plateau from global positioning system data, *Geology 32*(9), 809–812, doi:10.1130/G20554.1.

Zheng, Y., W. Zhou, P. A. Meyers, and S. Xie (2007), Lipid biomarkers in the Zoigê-Hongyuan peat deposit: Indicators of Holocene climate changes in West China, *Org. Geochem.*, *38*(11), 1927–1940, doi:10.1016/j.orggeochem.2007.06.012.